

Effect of residual stress on the delamination response of film-substrate systems under bending



P.J.J. Forschelen^a, A.S.J. Suiker^{a,*}, O. van der Sluis^{a,b}

^aEindhoven University of Technology, P.O. Box 513, NL-5600 MB, Eindhoven, The Netherlands

^bPhilips Research, High Tech Campus 34, NL-5656 AE, Eindhoven, The Netherlands

ARTICLE INFO

Article history:

Received 25 January 2016

Revised 28 May 2016

Available online 19 July 2016

Keywords:

Residual stress

Thin film delamination

Large scale yielding

Four-point bending test

Cohesive zone modelling

ABSTRACT

The effect of residual stress on the delamination behaviour of thin films is examined under four-point bending. Elastic film-substrate systems with and without the addition of a superlayer are analysed by constructing closed-form expressions for the energy release rate at steady-state delamination. The analytical results obtained with these expressions are compared to finite element results based on cohesive zone modelling, showing an excellent agreement. The closed-form expressions correctly reduce to simpler forms for film-substrate systems without residual stresses, and further include the special case of spontaneous delamination under the presence of a critical residual stress only. The closed-form expression for the elastic film-substrate system without a superlayer is used for indicating errors in alternative analytical expressions presented in the literature. Subsequently, the contribution of substrate plasticity to the delamination resistance is studied by means of finite element analyses for a range of (relative) film thicknesses and various values of the (relative) interfacial strength. For a compressive residual stress the delamination response typically is characterised by a transition from large scale yielding to small scale yielding under increasing film thickness, while for a tensile residual stress the limit of small scale yielding may not be reached at large film thickness when the interfacial strength is relatively high. Furthermore, stress relaxation induced by large scale yielding diminishes the influence of the residual stress on the delamination resistance under bending.

© 2016 Elsevier Ltd. All rights reserved.

1. Introduction

The delamination of thin films experiencing residual stresses plays an important role in a wide range of technological applications, including surface coatings, magnetic disks and integrated circuits. Residual stresses may originate from the deposition phase (intrinsic stresses), where they develop at the deposition temperature due to complex microstructural processes such as grain growth, defect annihilation, phase transitions, etc. (Freund and Suresh, 2003; Nix, 1989). Furthermore, they may be generated by a change in temperature (thermal stresses) when the film and substrate are characterised by different coefficients of thermal expansion. For certain film-substrate systems the magnitude of residual stresses can be in the order of several GPa's, leading to a substantial change of the driving force for interfacial delamination, or alternative modes of failure (Freund and Suresh, 2003).

The delamination resistance of thin films can be accurately measured in a four-point bending test, see Fig. 1, with the delami-

nation nucleating from a central notch and reaching a steady-state when its length a exceeds a few times the film thickness h_1 (Freund and Suresh, 2003; Hutchinson and Suo, 1992). Steady-state delamination develops under a constant bending moment (per unit width), $M = PL/2$, with $P/2$ the load (per unit width) and L the distance between the outer and inner loading lines. The steady-state conditions are preserved as long as the delamination remains between the inner loading lines, where the advance of delamination roughly follows from an equal mix of mode I (tension) and mode II (shear) when the thicknesses of the film and substrate are equal, but with the mode II contribution becoming more dominant at decreasing film thickness, and/or increasing elastic mismatch between film and substrate (Charalambides et al., 1989).

The delamination response of elastic film-substrate systems in four-point bending tests has been analysed in Charalambides et al. (1989); Hofinger et al. (1998); Hutchinson and Suo (1992); Klingbeil and Beuth (1997), and the effect of uniform residual stress has been included in Charalambides et al. (1990) and Delette et al. (2009). Several of these papers provide closed-form expressions for the energy release rate at steady-state delamination, which are compared to finite element results based on the

* Corresponding author. Fax: +31402450328.

E-mail address: a.s.j.suiker@tue.nl (A.S.J. Suiker).

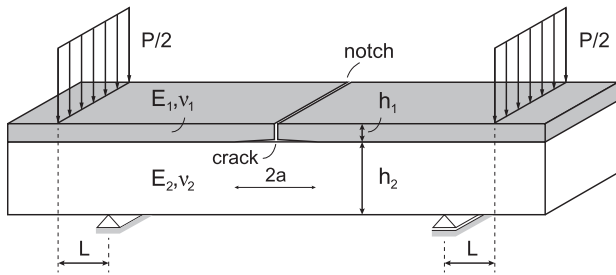


Fig. 1. Four-point bending test of a film (thickness h_1 and elastic properties E_1, ν_1) supported by a substrate (thickness h_2 and elastic properties E_2, ν_2). The delaminating crack between the film and substrate develops from a central notch under the applied couple (per unit width) $M = PL/2$.

computation of the J -integral (Rice, 1968). Although these comparisons generally led to a satisfactory agreement, it was observed that the closed-form expressions including the effect of residual stress, as presented in Charalambides et al. (1990) and Delette et al. (2009), show some noticeable differences. A comparison of these expressions with the closed-form expression derived in the present communication reveals that these mutual differences in fact are caused by errors in both expressions. This conclusion has been drawn after confirming the correctness of the present closed-form expression for various values of the residual stress through its excellent agreement with finite element results based on cohesive zone modelling. Here, the cohesive zone model uses the interface damage formulation presented in Cid Alfaro et al. (2009), which allows for a robust and accurate simulation of the mixed-mode delamination behaviour of thin films.

Motivated by the good agreement of the above-mentioned analytical and numerical results, a similar analysis is carried out for an elastic film-substrate system extended with a superlayer. By increasing the driving force for delamination, this modification of the film-substrate system ensures that for relatively high values of the interfacial fracture toughness alternative fracture events in the substrate are avoided, thus warranting an adequate measurement of the delamination response (Freund and Suresh, 2003). The closed-form expression for the steady-state energy release rate for thin film delamination reduces to simpler expressions presented in Klingbeil and Beuth (1997) and Hofinger et al. (1998) for the special case of zero residual stress, and also provides the critical residual stress for the occurrence of spontaneous delamination in the absence of bending.

The final configuration studied in this communication corresponds to an elastic film supported by an elasto-plastic (metal or polymer) substrate. Finite element analyses are performed for various ratios of the interfacial delamination strength and the yield strength of the substrate, showing that the delamination resistance under bending increases when the plastic dissipation at the delamination tip grows. Here, a compressive (tensile) residual stress increases (decreases) the delamination resistance. In the limit of zero delamination strength the finite element results reduce to a semi-analytical solution derived from a steady-state energy balance. A comparison of this solution with the steady-state solution for the elastic film-substrate system clearly indicates the transition from small scale yielding to large scale yielding under decreasing film thickness. Together with the analytical models for the elastic film-substrate systems, these numerical results can be effectively used for quantifying the contribution of the residual stress in the practical design against thin film delamination, and for the accurate determination of the delamination toughness from (four-point) bending experiments. The latter aspect is especially relevant in relation to the large variation in values typically measured for the interfacial toughness, ranging from 1 to 50 J/m²

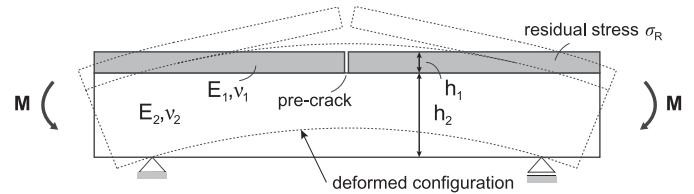


Fig. 2. Film-substrate system subjected to a couple M and a uniform residual stress σ_R in the film.

for polymer/metal and polymer/ceramic interfaces, and from 1 to 100 J/m² for metal/ceramic interfaces (Freund and Suresh, 2003; Wei and Hutchinson, 1997).

The paper is organized as follows. In Section 2 closed-form expressions are presented for the energy release rate for steady-state delamination in elastic film-substrate systems with and without a superlayer. Subsequently, a semi-analytical approach is outlined for the determination of the overall delamination resistance of elasto-plastic film-substrate systems that approach the limit of zero interfacial strength. Section 3 reviews the interface damage model adopted in the finite element analyses on thin film delamination, and discusses the geometry, boundary conditions and the finite element discretization. In Section 4 analytical and numerical results are presented for the steady-state delamination behaviour of various elastic and elasto-plastic film-substrate systems for a range of film-substrate thickness ratios. The section ends with comparing the overall four-point bend delamination responses of the various film-substrate systems considered in this communication. Section 5 provides some concluding remarks.

2. Steady-state delamination of thin films – analytical approach

The closed-form expressions that will be presented for the steady-state energy release rate for thin film delamination correspond to film-substrate systems subjected to bending, with a uniform residual stress present in the film. Steady-state delamination is typically reached when the delamination length exceeds a few times the film thickness (Freund and Suresh, 2003; Hutchinson and Suo, 1992). Accordingly, for a specific delamination toughness the closed-form expressions provide the critical bending moment for progressive delamination failure, and thus can be straightforwardly used to determine the delamination toughness from a four-point bending test. The expressions are further beneficial for validating the accuracy of spatial discretizations (meshes) of finite element models used for studying thin film delamination; illustrative examples thereof will be given in Section 4. The three systems considered in this communication are highly relevant for engineering practice, and are characterised by i) an elastic film supported by an elastic substrate, ii) an elastic film sandwiched between an elastic substrate and an elastic superlayer, and iii) an elastic film supported by an elasto-plastic substrate. In the analysis of the results in Section 4, special attention is focussed on the contribution of the film residual stress to delamination failure, an effect that is regularly ignored in the design against delamination.

2.1. Elastic film supported by an elastic substrate

Consider a simply-supported specimen composed of a thin film of thickness h_1 that is connected to a substrate of thickness h_2 , see Fig. 2. The elastic behaviour of the specimen is characterised by Young's moduli E_i and Poisson's ratios ν_i , with the indices $i = 1, 2$ representing the film and the substrate, respectively. At the specimen centre the film initially is pre-cracked in the vertical direction, and experiences a uniform residual stress σ_R caused by a mismatch

strain with the substrate. The specimen is loaded by an external couple M , representative of the conditions in a standard four-point bending test. When the bending moment M reaches a critical magnitude, the thin film will start to delaminate from the vertical pre-crack. After reaching steady-state conditions the energy release rate becomes independent of the length a of the delaminating crack (and further of the geometry of the initial pre-crack in the thin film from which the delamination nucleated). The energy released per unit advance of delamination can then be calculated from an energy balance incorporating the uncracked cross-section far ahead of the delamination tip ("upstream") and the cracked cross-section far behind the delamination tip ("downstream"), see also Beuth (1992); Ho and Suo (1993); Hutchinson and Suo (1992); Suiker and Fleck (2004),

$$\Delta W = \Delta F - \Delta U. \quad (1)$$

Here, ΔW is the interfacial energy consumed during delamination, ΔU is the difference in strain energy from the upstream and downstream cross-sections, and ΔF is the external work applied to the film-substrate specimen. Subsequently, the steady-state energy release rate G_{ss} follows as the interfacial energy dissipated per unit advance of delamination:

$$G_{ss} = \frac{\partial \Delta W}{\partial a}. \quad (2)$$

The determination of ΔU starts with the formulation of force and moment equilibrium across the upstream and downstream cross-sections, as characterised by the external couple M and the residual stress σ_R in the film. The solution computed for these equilibrium conditions results in the location of the neutral axis, which is used as input for the calculation of the corresponding strain energies. In addition, the external work ΔF is computed from the product of the bending moment M and the energetically-conjugated rotation that depends on the difference in curvature of the downstream and upstream cross-sections. Substituting the expressions for ΔU and ΔF , derived in Appendix A, in Eq. (1) leads with Eq. (2) to the following expression for the steady-state energy release rate:

$$G_{ss} = 6M^2 \left(\frac{1}{\bar{E}_2 h_2^3} - \frac{(\bar{E}_1 h_1 + \bar{E}_2 h_2)}{\xi} \right) + \frac{\sigma_R^2 \bar{E}_2 h_1 h_2 (\bar{E}_1 h_1^3 + \bar{E}_2 h_2^3) + 12\sigma_R M \bar{E}_1 h_1 \bar{E}_2 h_2 (h_1 + h_2)}{2\bar{E}_1 \xi}, \quad (3)$$

with the parameter ξ as

$$\xi = \bar{E}_1^2 h_1^4 + 4\bar{E}_1 h_1^3 \bar{E}_2 h_2 + 6\bar{E}_1 h_1^2 \bar{E}_2 h_2^2 + 4\bar{E}_1 h_1 \bar{E}_2 h_2^3 + \bar{E}_2^2 h_2^4, \quad (4)$$

and the plane-strain stiffness $\bar{E}_i = E_i / (1 - \nu_i^2)$, with the indices $i = 1, 2$ representing the film and the substrate, respectively. More details of the above derivation procedure can be found in Appendix A. Note that Eq. (3) is composed of three parts, namely a part related to the bending moment M , a part related to the residual stress σ_R in the film, and a part related to the coupling of M and σ_R . When the residual stress is absent, $\sigma_R = 0$, Eq. (3) simplifies to the expression for the energy release rate under pure bending:

$$G_{ss} = 6M^2 \left(\frac{1}{\bar{E}_2 h_2^3} - \frac{(\bar{E}_1 h_1 + \bar{E}_2 h_2)}{\xi} \right), \quad (5)$$

with the parameter ξ given by Eq. (4). The reduced form, Eq. (5), has been reported previously by other authors (Charalambides et al., 1990; 1989; Hutchinson and Suo, 1992).

2.2. Elastic film-substrate system with an additional elastic superlayer

The second system considered consists of a film-substrate system that is extended with a superlayer of thickness h_s , see

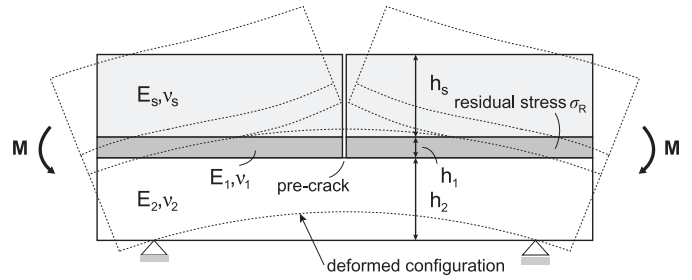


Fig. 3. Film-substrate system with an additional superlayer of thickness h_s and elastic properties E_s , ν_s , which is subjected to a couple M and a uniform residual stress σ_R in the film.

Fig. 3. As for the basic film-substrate configuration introduced in Section 2.1, the system experiences a uniform residual stress in the film and is subjected to an external couple M . The addition of a superlayer may be necessary if the maximum tensile stress generated in the substrate reaches its tensile strength, such that vertical cracks develop before interfacial delamination can occur. The configuration with an additional superlayer indeed may reverse the order of cracking by increasing the driving force for delamination or may prevent cracking of brittle thin films. The superlayer system was used in Zhuk et al. (1998) to examine the interfacial toughness of a metal film on a polymeric substrate, and in Bagchi et al. (1994) to investigate delamination of Cu thin films on silica substrates. In Hofinger et al. (1998), this configuration was applied for measuring the interface fracture energy of a ZrO_2 -ceramic layer on a high-alloyed steel substrate.

The steady-state energy release rate of this system is computed in the same fashion as for the basic film-substrate system presented in Section 2.1. However, the strain energy of the downstream cross-section now depends on an additional component that can be attributed to the curvature induced in the film and the superlayer. This curvature is caused by the residual stress in the film and the constraint following from the coherent interface between the film and superlayer. The expression for the energy release rate for delamination depends on the geometric parameters (h_1 , h_2 , h_s), the plane-strain elastic material properties (\bar{E}_1 , \bar{E}_2 , \bar{E}_s), the loading parameters (M , σ_R), and has the form

$$G_{ss} = 6M^2 \left(\frac{1}{\bar{E}_2 h_2^3} - \frac{(\bar{E}_1 h_1 + \bar{E}_2 h_2 + \bar{E}_s h_s)}{\gamma} \right) + \frac{\sigma_R^2 h_1}{2\bar{E}_1} \left(\frac{-3\bar{E}_1 h_1 [h_1 (\bar{E}_2 h_2 - \bar{E}_s h_s) + \bar{E}_2 h_2^2 - \bar{E}_s h_s^2]^2 + \gamma (\bar{E}_2 h_2 + \bar{E}_s h_s)}{(\bar{E}_1 h_1 + \bar{E}_2 h_2 + \bar{E}_s h_s) \gamma} - \frac{\bar{E}_s h_s (\bar{E}_1 h_1^3 + \bar{E}_s h_s^3)}{\beta} \right) + 6\sigma_R M h_1 \left(\frac{h_1 (\bar{E}_2 h_2 - \bar{E}_s h_s) + \bar{E}_2 h_2^2 - \bar{E}_s h_s^2}{\gamma} \right), \quad (6)$$

with the parameters β and γ given by

$$\begin{aligned} \beta &= \bar{E}_1^2 h_1^4 + 4\bar{E}_1 h_1^3 \bar{E}_s h_s + 6\bar{E}_1 h_1^2 \bar{E}_s h_s^2 + 4\bar{E}_1 h_1 \bar{E}_s h_s^3 + \bar{E}_s^2 h_s^4, \\ \gamma &= \bar{E}_1^2 h_1^4 + 4\bar{E}_1 h_1^3 (\bar{E}_2 h_2 + \bar{E}_s h_s) \\ &\quad + h_1^2 [(6\bar{E}_1 h_2^2 + 12\bar{E}_s h_2 h_s) \bar{E}_2 + 6\bar{E}_1 \bar{E}_s h_s^2] \\ &\quad + h_1 [4h_2 (3h_s (h_2 + h_s) \bar{E}_s + \bar{E}_1 h_2^2) \bar{E}_2 + 4\bar{E}_1 \bar{E}_s h_s^3] + \bar{E}_2^2 h_2^4 \\ &\quad + 4\bar{E}_2 h_2 \bar{E}_s h_s \left(h_2^2 + \frac{3}{2} h_2 h_s + h_s^2 \right) + \bar{E}_s^2 h_s^4. \end{aligned} \quad (7)$$

As for the film-substrate system without the superlayer, the energy release rate consists of a component related to the couple M , a component due to the residual stress σ_R in the film, and a part depending on the coupling of M and σ_R . It can be confirmed that Eq. (6) reduces to the steady-state energy release rate for the film-substrate system, Eq. (3), if the superlayer thickness h_s is set to

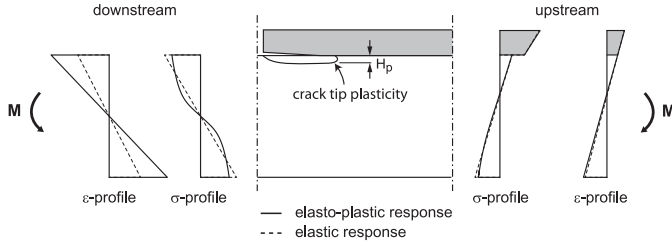


Fig. 4. Elastic film supported by an elasto-plastic substrate that is subjected to a couple M . During film delamination two types of plastic zones can be distinguished: i) bulk plasticity at the downstream cross-section (and also, but to a lesser extent, at the upstream cross-section) and ii) local plasticity at the crack tip (indicated by a trail of plastically deformed material of size H_p). The upstream and downstream stress and strain profiles are sketched qualitatively for the case of an elastic substrate (dashed line) and for an elasto-plastic substrate (solid line).

zero. In addition, when the residual stress is absent, $\sigma_R = 0$, the energy release rate for delamination in a three-layer system subjected to bending is obtained:

$$G_{ss} = 6M^2 \left(\frac{1}{\bar{E}_2 h_2^3} - \frac{(\bar{E}_1 h_1 + \bar{E}_2 h_2 + \bar{E}_s h_s)}{\gamma} \right). \quad (8)$$

This reduced equation was reported previously in Hofinger et al. (1998); Klingbeil and Beuth (1997).

2.2.1. Symmetric composite configuration

It is common practice to create three-layer systems by gluing together two film-substrate systems, with the film faces oriented towards each other. For this system the superlayer and substrate have the same height, $h_s = h_2$, and elastic properties, $\bar{E}_s = \bar{E}_2$. The two films of thickness h_1 glued together act as *one film* of thickness $2h_1$, which is subjected to a residual stress σ_R . Accordingly, the energy release rate for this system can be derived from Eq. (6) as

$$G_{ss} = 6M^2 \left(\frac{1}{\bar{E}_2 h_2^3} - \frac{1}{8 \bar{E}_1 h_1^3 + (3h_1^2 h_2 + 3h_1 h_2^2 + h_2^3) \bar{E}_2} \right) + \frac{\sigma_R^2 h_1 h_2 \bar{E}_2}{\bar{E}_1} \left(\frac{1}{\bar{E}_1 h_1 + \bar{E}_2 h_2} - \frac{8\bar{E}_1 h_1^3 + \bar{E}_2 h_2^3}{16\bar{E}_1^2 h_1^4 + 32\bar{E}_1 h_1^3 \bar{E}_2 h_2 + 24\bar{E}_1 h_1^2 \bar{E}_2 h_2^2 + 8\bar{E}_1 h_1 \bar{E}_2 h_2^3 + \bar{E}_2^2 h_2^4} \right). \quad (9)$$

with h_1 thus referring to *half* of the film thickness. Observe from Eq. (9) that the coupling term for the residual stress σ_R and the moment M has disappeared from the expression. When the residual stress vanishes ($\sigma_R = 0$) and the deformation of the film material is neglected (thus taking $h_1 = 0$), Eq. (9) reduces to

$$G_{ss} = \frac{21M^2}{4\bar{E}_2 h_2^3}, \quad (10)$$

which has been presented previously in Freund and Suresh (2003); Shaviv et al. (2005).

2.3. Elastic film supported by an elasto-plastic substrate

The third system considered is composed of an elastic film supported by an elasto-plastic substrate, as sketched in Fig. 4. Because the plastic deformations are restricted to the substrate, prior to delamination these need to be accommodated by elastic deformations in the film. Apart from the energy ΔW dissipated by interfacial delamination, the steady-state energy balance for this system also includes the dissipation ΔD related to plasticity, i.e.,

$$\Delta W + \Delta D = \Delta F - \Delta U. \quad (11)$$

Consequently, the energy originally available for thin film delamination is lowered by the amount of plastic dissipation ΔD . This dissipation term in principle may include the effects of bulk plasticity across the upstream and downstream cross-sections of the substrate, as well as local plastic effects near the delamination tip. More specifically, local plasticity is developed in the wake of the delaminating crack by a trail of plastically deformed but partially unloaded material, of which the size H_p at a certain delamination becomes constant thereby reaching a steady state (Freund and Suresh, 2003; Tvergaard and Hutchinson, 1992; 1993; Wei and Hutchinson, 1997). Fig. 4 illustrates this local plastic effect, together with the stress and strain profiles at the plastically deformed upstream and downstream cross-sections. Under an increasing bending moment M the unloading effects at these remote cross-sections are negligible, so that the corresponding stresses and strains monotonically increase. Accordingly, the deformation theory of plasticity may be applied, whereby the elasto-plastic behaviour at the upstream and downstream cross-sections is described by a non-linear elastic constitutive model. This contribution can be conveniently incorporated in the energy balance, Eq. (11), through the difference in strain energy ΔU , instead of the plastic dissipation ΔD . The plastic dissipation ΔD then only includes local plastic deformation effects produced near the crack tip.

As demonstrated in Cid Alfaro et al. (2009); Tvergaard and Hutchinson (1992, 1993); Wei and Hutchinson (1997), the local plastic deformations generated near the crack tip strongly depend on the ratio between the ultimate fracture strength t^u and the (tensile) yield strength σ_y of the adjacent bulk material (i.e., the substrate material). In the limit case of the relative fracture strength approaching to zero, $t^u/\sigma_y \rightarrow 0$, local plastic dissipation near the crack tip will vanish, $\Delta D \rightarrow 0$, and the film-substrate system will only experience bulk plasticity across the height of the substrate. The steady-state energy balance, Eq. (11), then obtains the same form as for the elastic film-substrate system, Eq. (1), so that the energy release rate for steady-state delamination may be computed with a similar procedure as outlined in Section 2.1. Note, however, that the steady-state energy release rate for the limit case of $t^u/\sigma_y \rightarrow 0$ has limited practical value, since the manufacturing of film-substrate systems with relatively weak interfaces typically is avoided because of the high susceptibility to delamination failure. Nonetheless, it is interesting to explore the validity range of this steady-state solution as an approximation for the delamination response of film-substrate systems with finite interfacial strength. In addition, this solution can be compared against the solution derived for the elastic film-substrate system, in order to highlight the contribution of bulk plasticity to steady-state delamination failure. Moreover, it serves as a convenient tool for validating the accuracy of the spatial discretization in FEM models of film-substrate systems. The benefit of the semi-analytical solution with respect to these three aspects is clearly demonstrated in the analysis of the results in Section 4.3. In the subsequent section several features of the plasticity formulation are summarised.

2.3.1. Plasticity formulation

The elasto-plastic material response is characterised in accordance with the Ramberg–Osgood relation (Ramberg and Osgood, 1943)

$$\varepsilon_m = \frac{\sigma_m}{E} + \alpha \frac{\sigma_m}{E} \left(\frac{\sigma_m}{\sigma_y} \right)^{N-1}, \quad (12)$$

where ε_m and σ_m formally are interpreted as the uniaxial strain and stress, respectively, E is Young's modulus, σ_y is the yield strength, and α and N are parameters describing the specific hardening behaviour of the material. The above uniaxial constitutive

relation can also be used for multiaxial loading conditions, by taking σ_m and ε_m as equivalent stress and strain measures, respectively. These equivalent measures commonly are chosen in accordance with a von Mises formulation, which, under plane-strain conditions (with the z -direction taken as the out-of-plane direction), leads to the following expressions for the normal stress σ_{xx} and strain ε_{xx} in the axial direction of the film-substrate system (see Appendix B for more details):

$$\sigma_{xx} = \frac{\sigma_m}{\sqrt{\nu_s^2 - \nu_s + 1}},$$

$$\varepsilon_{xx} = \frac{(\nu_s + 1)}{2} \left(\frac{-\nu_s}{E_s} \sigma_{xx} + \sqrt{4\varepsilon_m^2 - \frac{3\nu_s^2}{E_s^2} \sigma_{xx}^2} \right). \quad (13)$$

Here, $E_s = \sigma_m/\varepsilon_m$ is the secant stiffness of the elasto-plastic material and $\nu_s = 1/2 - (1/2 - \nu)E_s/E$ is the corresponding Poisson's ratio, whereby E and ν are the Young's modulus and Poisson's ratio of a linear elastic material.

As for the elastic film-substrate system, the location of the neutral axis under the application of a couple M and the presence of a residual stress σ_R is computed by considering force and moment equilibrium at the upstream and downstream cross-sections. However, due to the nonlinear stress distribution across the substrate height caused by plasticity, this procedure needs to be performed in an iterative (numerical) fashion, which is done by discretizing the cross-section of the substrate in a specific number of equal-sized cells across its height. Under the initial assumption of a linear distribution of the equivalent stress σ_m across the system height, for each substrate cell the corresponding equivalent strain ε_m is computed through Eq. (12), which leads to the corresponding normal stress σ_{xx} and strain ε_{xx} by means of Eq. (13). In addition, for the thin film the normal strain straightforwardly follows from the assumed stress through its linear elastic behaviour. The corresponding forces and moments at the cross-sections are computed from a summation of the contributions of the individual cells, and equilibrium is enforced iteratively by using a Newton-Raphson algorithm. This procedure typically converges after a few iterative updates of the equivalent stresses σ_m in the cells. The final (converged) location of the neutral axis is used for determining the strain energy difference ΔU from the upstream and downstream cross-sections, which then provides the steady-state energy release rate for delamination through Eqs. (2) and (11), with local plasticity near the delamination tip thus being left out of consideration ($\Delta D = 0$).

3. Numerical model

The various film-substrate systems introduced in the previous section are simulated for a broad range of structural and material parameters by using the finite element method (FEM). This section treats the interface damage model adopted for describing the delamination behaviour of the film, and provides information on the geometry, boundary conditions and spatial discretization used in the numerical simulations.

3.1. Review of the interface damage model

The film-substrate configurations are modelled with the aid of the finite element program ABAQUS Standard¹, where the delamination behaviour of the thin film is simulated with interface elements. The interface elements are endowed with the mixed-mode damage model presented in Cid Alfaro et al. (2009), which has been included in ABAQUS as a user-supplied material subroutine

(i.e., a 'UMAT'). In Cid Alfaro et al. (2009) this interface damage model was successfully applied for a three-dimensional analysis of a basic laminate failure mechanism characterised in Suiker and Fleck (2004; 2006). The model further has been used for the numerical simulation of complex fracture patterns in thin fiber-epoxy layers, describing both decohesion at fibre-epoxy interfaces and matrix cracking in the epoxy in a robust and accurate fashion (Cid Alfaro et al., 2010a; 2010b). For clarity reasons, the main equations of the interface damage model are reviewed below, whereby the general three-dimensional formulation presented in Cid Alfaro et al. (2009) is reduced to a two-dimensional formulation, in correspondence with the plane-strain analyses performed in the present work. Accordingly, the constitutive equation expressing the tractions \mathbf{t} in terms of the relative displacements \mathbf{v} across an interface is given in component form as

$$t_i = (1 - d)Kv_i - dK\delta_{ii}\langle -v_1 \rangle \quad \text{with} \quad i \in \{1, 2\}, \quad (14)$$

where the normal and tangential components of the tractions and relative displacements are indicated by the indices '1' and '2', respectively. Additionally, K is the elastic interfacial stiffness (dimension is force \times length⁻³) and δ_{ij} is the Kronecker delta symbol. The damage parameter d is bounded as $0 \leq d \leq 1$, with an undamaged material point represented by $d = 0$ and a fully damaged material point reflected by $d = 1$. The penetration of two opposite crack faces is avoided by the second term in the right-hand side of Eq. (14), with the Macauley brackets $\langle x \rangle = \frac{1}{2}(x + |x|)$ warranting that crack faces are in elastic contact when the normal relative displacement v_1 becomes negative. For generality, the damage evolution occurs in a rate-dependent fashion, with the rate of damage given by

$$\dot{d} = \begin{cases} \frac{\hat{F}_d(\lambda_d, \kappa_d)}{\eta_d} & \text{for} \quad \lambda_d \geq \kappa_d \quad \text{and} \quad v^0 \leq \kappa_d < v^\mu, \\ 0 & \text{for} \quad 0 \leq \lambda_d < \kappa_d \quad \text{or} \quad \kappa_d = v^\mu. \end{cases} \quad (15)$$

Here, η_d is the damage relaxation parameter (with dimension of time) and $\hat{F}_d(\lambda_d, \kappa_d)$ is the damage loading function, which depends on a deformation measure λ_d and a damage history variable κ_d . The deformation measure λ_d is supposed to be equal to the Euclidean norm of the vector of relative crack face displacements, $\lambda_d = \|\mathbf{v}\| = \sqrt{v_1^2 + v_2^2}$. The upper expression in Eq. (15) defines the rate of damage when the effective deformation λ_d surpasses the value of the damage history variable κ_d , whereas the lower expression sets the rate of damage equal to zero when (i) the threshold value for damage nucleation has not (yet) been reached, (ii) the interfacial material point experiences unloading, or (iii) the interfacial material point has been fully damaged. As illustrated by Eq. (15), the damage history variable is limited by the range $v^0 \leq \kappa_d \leq v^\mu$, with v^0 and v^μ the relative crack face displacements at the onset of damage ($d = 0$) and damage completion ($d = 1$), respectively.

The specific form of the damage loading function $\hat{F}_d(\lambda_d, \kappa_d)$ depends on the shape of the softening branch in the traction-separation relation. Fig. 5 illustrates that damage growth in the present study is characterised by a linear softening branch, which results in the following damage loading function:

$$F_d = \hat{F}_d(\lambda_d, \kappa_d) = \hat{f}(\lambda_d) - \hat{d}(\kappa_d) = \frac{v^\mu(\lambda_d - v^0)}{\lambda_d(v^\mu - v^0)} - \frac{v^\mu(\kappa_d - v^0)}{\kappa_d(v^\mu - v^0)}. \quad (16)$$

Note from Eq. (15) that in the limit case of the damage relaxation parameter approaching to zero, $\eta_d \rightarrow 0$, the rate-independent loading condition: $\hat{F}_d(\lambda_d, \kappa_d) = 0$ is recovered, which, as can be concluded from Eq. (16), corresponds to $\lambda_d = \kappa_d$.

¹ Hibbitt, Karlsson & Sorensen, Inc., Pawtucket, RI, U.S.A.

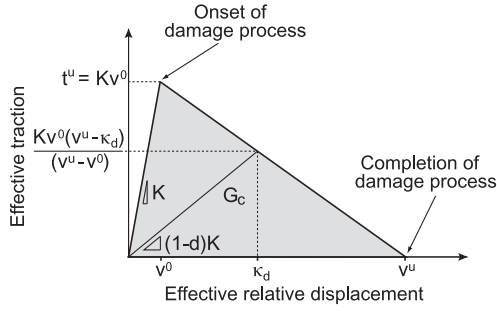


Fig. 5. Traction-separation law (taken from Cid Alfaro et al. (2009)).

In order to simulate fracture processes of arbitrary mode-mixity, the relative displacements at damage initiation, v^0 , and damage completion, v^u , need to be made dependent on a mode-mixity parameter β , see also Turon et al. (2006):

$$\beta = \frac{|v_2|}{|v_2| + \langle v_1 \rangle}. \quad (17)$$

Eq. (17) shows that under pure mode I (tensile) loading conditions $\beta = 0$ (since $v_2 = 0$), and under pure mode II (shear) loading conditions $\beta = 1$ (since $v_1 = 0$). The functions $v^0 = \hat{v}^0(\beta)$ and $v^u = \hat{v}^u(\beta)$ are constructed by invoking an energy-based, mixed-mode failure criterion from linear elastic fracture mechanics, see Cid Alfaro et al. (2009); Turon et al. (2006). Accordingly, a criterion regularly used for quantifying mixed-mode toughness data for brittle interfacial fracture is adopted (Hutchinson and Suo, 1992; Jensen, 1990):

$$\frac{G_I}{G_{I,c}} + \frac{G_{II}}{G_{II,c}} = 1. \quad (18)$$

Here, G_I and G_{II} are the mode I and mode II energy release rates, and $G_{I,c}$ and $G_{II,c}$ are the toughnesses under pure mode I and pure mode II loading conditions respectively. With the use of Eqs. (17) and (18) the effective relative displacements at damage nucleation and damage completion can be, respectively, derived as

$$v^0 = \hat{v}^0(\beta) = v_1^0 v_2^0 \sqrt{\frac{1 + 2\beta^2 - 2\beta}{(\beta v_1^0)^2 + ((1 - \beta)v_2^0)^2}}, \quad (19)$$

and

$$v^u = \hat{v}^u(\beta) = \frac{2(1 + 2\beta^2 - 2\beta)}{K v^0} \left[\left(\frac{(1 - \beta)^2}{G_{I,c}} \right) + \left(\frac{\beta^2}{G_{II,c}} \right) \right]^{-1}, \quad (20)$$

where $v_1^0 = t_1^u/K$ and $v_2^0 = t_2^u/K$ are the relative displacements at which damage nucleates under pure mode I and pure mode II loading conditions, respectively, and t_1^u and t_2^u are the ultimate tractions under pure mode I and pure mode II conditions, respectively.

Details of the numerical implementation of the above damage model can be found in Cid Alfaro et al. (2009). The numerical implementation is based on an implicit (backward Euler) scheme and uses a consistent tangent operator. The update algorithm is relatively straightforward, stable and fast, since it does not require numerical iterations; these aspects can be ascribed to the specific form of the damage loading function used, Eq. (16).

3.2. Geometry, boundary conditions and finite element discretization

In the finite element simulations the film-substrate systems were subjected to plane-strain conditions, whereby delamination was generated through the application of a couple M and the presence of a residual stress σ_R in the film. The couple M was activated in a set-up mimicking a four-point bending test, by incrementally

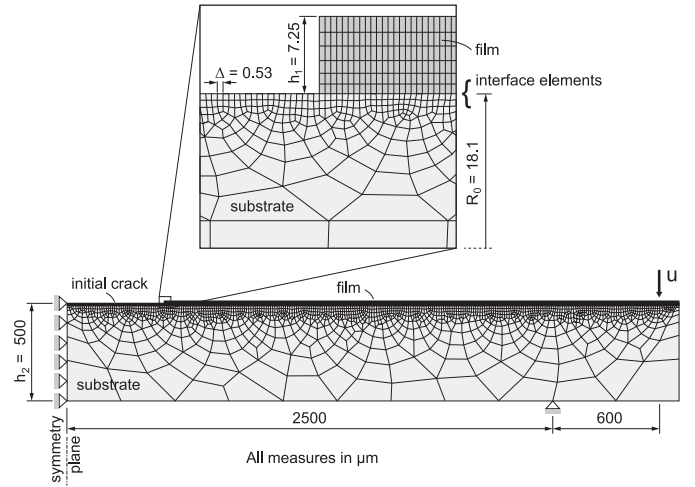


Fig. 6. Finite element mesh for a film-substrate system subjected to four-point bending (through applying a vertical displacement u out the outer loading line), with typical values indicated for the local mesh size Δ , the film thickness h_1 , the substrate thickness h_2 , the size R_0 of the plastic zone at the delamination tip, the distance between the inner and outer loading lines (600 μm), and the half-span of the specimen (2500 μm).

applying a vertical displacement u at a distance L outside the vertical supports of the specimen. The energetically-conjugated force $P/2$ (per unit specimen width) corresponding to this vertical displacement, multiplied by the distance L , provides the bending moment, $M = PL/2$ (per unit width). For the three film-substrate systems introduced in Sections 2.1–2.3, it is assumed that the film delaminates symmetrically from a vertical pre-crack at the centre of the specimen. Accordingly, half of the specimen was meshed, and roller supports were applied to warrant symmetry and to prevent rigid body motions, see Fig. 6. The pre-crack from which the delamination nucleates was modelled by leaving out the film layer over a small distance near the centre of the specimen. The specific value of this distance does not strongly affect the delamination response characteristics; steady-state delamination is reached after the crack has developed over a relatively small length, equal to a few times the film thickness. The value of the residual stress σ_R in the film was explicitly prescribed at the onset of the simulation as an initial condition; subsequently, the residual stress was allowed to relax over a single time step, before the application of the bending moment M .

The numerical analyses were performed within a small-displacement, small-strain framework; comparisons with finite strain simulations showed that for the (quasi-) brittle systems examined in this work the difference in failure response is negligible, which justifies the assumption of small strains and displacements. The loading rate was kept sufficiently small to mimic quasi-static loading conditions. The film-substrate systems considered were modelled using plane-strain 8-node iso-parametric elements, with a 3×3 Gauss quadrature. The interface along which delamination occurs was modelled using 4-node interface elements equipped with a 2-point Gauss quadrature. Connecting a side of a quadratic plane-strain continuum element to two linear interface elements formally introduces a small incompatibility between the displacement fields of both element types; however, this incompatibility becomes negligible when applying a very fine mesh. As illustrated in Fig. 6, the finite element mesh indeed was chosen relatively fine near the material interface, also for accurately capturing the stress concentration at the delamination tip. The continuum elements at the interface are approximately square-shaped, having a size Δ . It is required that Δ is small enough to accurately describe the local failure response at the process zone of the delamination tip.

For the fracture problems studied in [Chen et al. \(2001\)](#); [Cid Alfaro et al. \(2009\)](#); [Tvergaard and Hutchinson \(1992\)](#), convergence of the finite element results upon mesh refinement was found if the size Δ was chosen smaller than about 4 times the ultimate separation ν^μ in the traction-separation law (see [Eq. \(20\)](#) and [Fig. 5](#) for the definition of ν^μ). Accordingly, for the simulations performed in this communication the element size near the interface was chosen as $\Delta \approx 2\nu^\mu$, for which convergence of the numerical results indeed could be confirmed from a mesh refinement study.

For the FEM simulations of a thin film supported by an elasto-plastic substrate, the elasto-plastic material response was modelled with the Ramberg–Osgood model, [Eq. \(12\)](#), using a *flow plasticity formulation* with a von Mises yield criterion. For the analysis of the results, the plastic zone developing near the delamination tip was estimated by means of a material-based length scale parameter R_0 ([Tvergaard and Hutchinson, 1992; 1993; Wei and Hutchinson, 1997](#)):

$$R_0 = \frac{1}{3\pi} \frac{\bar{E}_2 G_c}{\sigma_y^2}, \quad (21)$$

where \bar{E}_2 denotes the plane-strain modulus of the substrate, G_c is the interface toughness, and σ_y is the yield stress of the substrate material. [Eq. \(21\)](#) estimates the height of the plastic zone for the case of a film delaminating from a semi-infinite substrate under mode I loading conditions, thereby assuming the plastic dissipation at the crack tip to remain small. As demonstrated in [Tvergaard and Hutchinson \(1992, 1993\)](#); [Wei and Hutchinson \(1997\)](#), it is insightful to adopt R_0 as an essential variable in a parametric analysis of thin film delamination. The magnitude of R_0 , together with the length scale ν^μ characterising the size of the cohesive zone at the delamination tip, also dictates the minimal mesh size required for obtaining accurate numerical results. In the simulations performed in the present communication, the size of the plastic zone R_0 typically is (much) larger than the magnitude of ν^μ , so that ν^μ was most decisive in the determination of the minimal mesh size near the delaminating material interface. For obtaining an accurate description of the plastic zone over the full delamination length, near the material interface a large number of relatively small elements needed to be applied. Accordingly, depending on the film thickness, the elastic configurations comprise 10,000 to 20,000 elements, and the elasto-plastic configurations consist of 15,000 to 60,000 elements. Preliminary simulations indicated that these meshes also appear to be sufficiently fine to avoid volumetric locking during isochoric plastic deformation.

4. Discussion of results

In the present section the steady-state delamination response is analysed for the three film-substrate systems introduced in [Sections 2.1–2.3](#). Analytical results obtained with the closed-form expressions are compared against FEM results. Additional FEM results are presented for the case of an elastic film delaminating from an elasto-plastic substrate.

4.1. Elastic film supported by an elastic substrate

Consider the elastic film-substrate system shown in [Fig. 2](#). For an optimal presentation of the results, the expression for the steady-state energy release rate, [Eq. \(3\)](#), is rewritten in terms of the relative height $\lambda = h_2/h_1$, and the stiffness mismatch between the substrate and the film, $R = \bar{E}_2/\bar{E}_1$. The Poisson's ratios of the film and substrate are assumed to be equal, $\nu_1 = \nu_2 = 0.3$. Note that the expressions for the present plane-strain model can also be applied for *plane-stress conditions* by using a stiffness mismatch $R = E_2/E_1$ instead. The steady-state energy release rate G_{ss} is decomposed in a contribution $G_{M,ss}$ due to the applied couple M , a contribution

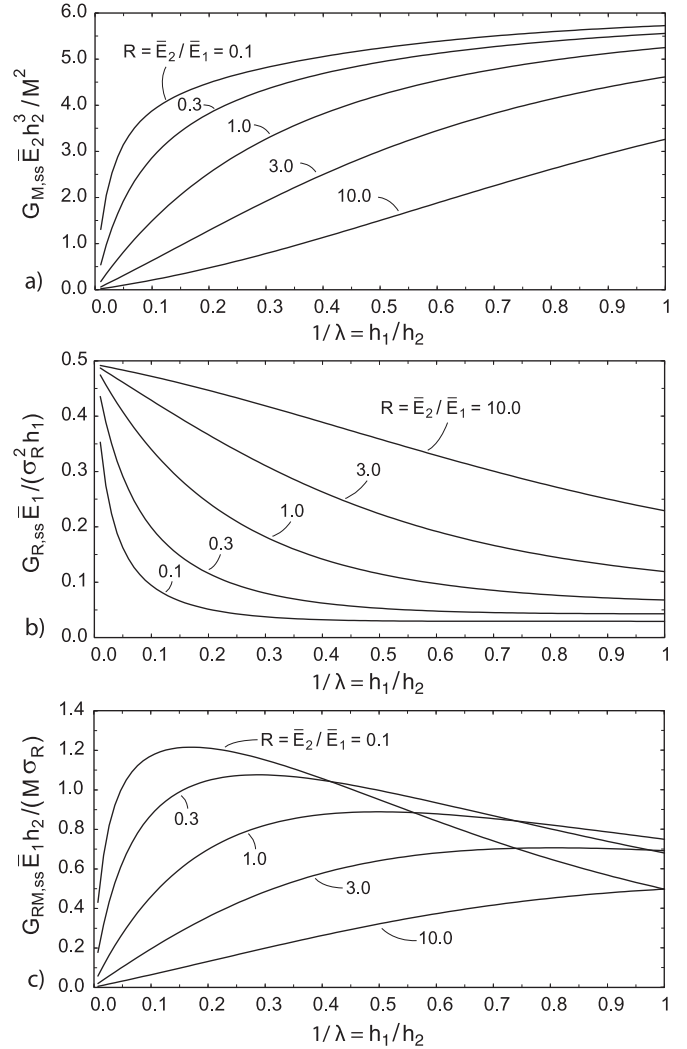


Fig. 7. Elastic film-substrate system: Three components of the steady-state energy release rate for delamination, G_{ss} , as a function of the relative film thickness, h_1/h_2 , for different stiffness ratios, $R = \bar{E}_2/\bar{E}_1$. a) Component $G_{M,ss}$ due to the applied couple M . b) Component $G_{R,ss}$ due to the residual stress σ_R . c) Component $G_{RM,ss}$ due to the coupling of σ_R and M .

$G_{R,ss}$ due to the residual stress σ_R in the film, and a contribution $G_{RM,ss}$ due to the coupling of the bending moment and the residual stress:

$$G_{ss} = G_{M,ss} + G_{R,ss} + G_{RM,ss}, \quad (22)$$

with the three individual components as

$$\begin{aligned} G_{M,ss} &= \frac{6M^2}{\bar{E}_2 h_2^3} \left(\frac{3R\lambda(1+\lambda)^2 + (1+R\lambda)}{3R\lambda(1+\lambda)^2 + (1+R\lambda)(1+R\lambda^3)} \right), \\ G_{R,ss} &= \frac{\sigma_R^2 h_1}{2\bar{E}_1} \left(\frac{R\lambda(1+R\lambda^3)}{3R\lambda(1+\lambda)^2 + (1+R\lambda)(1+R\lambda^3)} \right), \\ G_{RM,ss} &= \frac{6M\sigma_R}{\bar{E}_1 h_2} \left(\frac{R\lambda^2(1+\lambda)}{3R\lambda(1+\lambda)^2 + (1+R\lambda)(1+R\lambda^3)} \right). \end{aligned} \quad (23)$$

4.1.1. Components of the energy release rate

The components presented in [Eq. \(23\)](#) are plotted in dimensionless form in [Fig. 7](#) as a function of the relative film thickness $\lambda^{-1} = h_1/h_2$, for different values of the stiffness mismatch R . [Fig. 7](#) illustrates that for a higher film stiffness (reflected by a lower value of R) the value of $G_{M,ss}$ generally *increases*. The increase

in film stiffness enlarges the film bending stress and its contribution to the upstream strain energy, as a result of which the drop in strain energy from the upstream (film + substrate) to downstream (only substrate) cross-sections becomes larger and the delamination driving force $G_{M,ss}$ grows. For the same reason, $G_{M,ss}$ increases under increasing relative film thickness h_1/h_2 , whereby in the limit of an infinite film thickness, $h_1/h_2 \rightarrow \infty$, all curves asymptote towards the same value, $G_{M,ss}\bar{E}_2h_2^3/M^2 = 6$. The curves in Fig. 7a are in correspondence with those plotted in Fig. 3 of Charalambides et al. (1989), in which film delamination was analysed under bending but without the presence of a residual stress in the film.²

In contrast to the above trend, the value of $G_{R,ss}$ decreases when the film stiffness increases and/or the film thickness becomes larger, see Fig. 7b. This is, because the distance between the line of action of the resultant force of the film residual stress (located at half of the film thickness) and the neutral axis at the upstream cross-section becomes smaller, whereby the contribution from the residual stress to the drop in strain energy decreases and $G_{R,ss}$ reduces. In the limit of $h_1/h_2 \rightarrow \infty$ this distance goes to zero, as a result of which the normalised energy release rate asymptotes to $G_{R,ss}\bar{E}_1/(\sigma_R^2h_1) = 0$ for arbitrary stiffness mismatches R .

For the coupling term $G_{RM,ss}$ the two effects described above are in competition, whereby for a relatively small film thickness the effect by the applied bending moment prevails, with a stiffer film leading to a higher energy release rate. However, for higher film thicknesses the reducing effect on the energy release rate by the residual stress starts to become important, causing the curves for low stiffness ratios R to reach a maximum, after which they decrease and cross the curves for the higher stiffness ratios (thereby changing the order of appearance). In contrast to the terms $G_{M,ss}$ and $G_{R,ss}$ that always have positive values, the coupling term G_{RM} can obtain both positive and negative values. Since in a four-point bending test the couple M applied for generating film delamination is always positive (using a right-handed coordinate system with the positive y-axis pointing downwardly, see Fig. A.1 in Appendix A), a negative coupling term is associated to a compressive residual stress in the film.

4.1.2. Effect of residual stress on energy release rate

In order to examine the effect of the residual stress on the total steady-state energy release rate, a dimensionless loading parameter τ is introduced as

$$\tau = \frac{\sigma_R}{\sigma_M} \quad \text{with} \quad \sigma_M = 6M/h_2^2, \quad (24)$$

where σ_M may be interpreted as the maximum (tensile) bending stress at the downstream (delaminated) cross-section of the system. Inserting Eq. (24) into Eq. (23) leads to the following expressions for the three components of the energy release rate:

$$\begin{aligned} \frac{G_{M,ss}\bar{E}_2h_2^3}{M^2} &= 6 \left(\frac{3R\lambda(1+\lambda)^2 + (1+R\lambda)}{3R\lambda(1+\lambda)^2 + (1+R\lambda)(1+R\lambda^3)} \right), \\ \frac{G_{R,ss}\bar{E}_2h_2^3}{M^2} &= 18\tau^2 \left(\frac{R^2(1+R\lambda^3)}{3R\lambda(1+\lambda)^2 + (1+R\lambda)(1+R\lambda^3)} \right), \\ \frac{G_{RM,ss}\bar{E}_2h_2^3}{M^2} &= 36\tau \left(\frac{R^2\lambda^2(1+\lambda)}{3R\lambda(1+\lambda)^2 + (1+R\lambda)(1+R\lambda^3)} \right). \end{aligned} \quad (25)$$

Fig. 8a depicts the steady-state energy release rate G_{ss} (in dimensionless form) as a function of the relative film thickness h_1/h_2 , for

² It is noted that in Charalambides et al. (1989) the chosen dimensionless form of the energy release rate, as depicted on the vertical axis of Fig. 3, differs by a factor $4((h_1 + h_2)/h_2)^3$ from the form chosen in Fig. 7a, where the factor of 4 follows from normalizing the energy release rate by the square of the moment PL instead of the square of the applied moment $M = PL/2$.

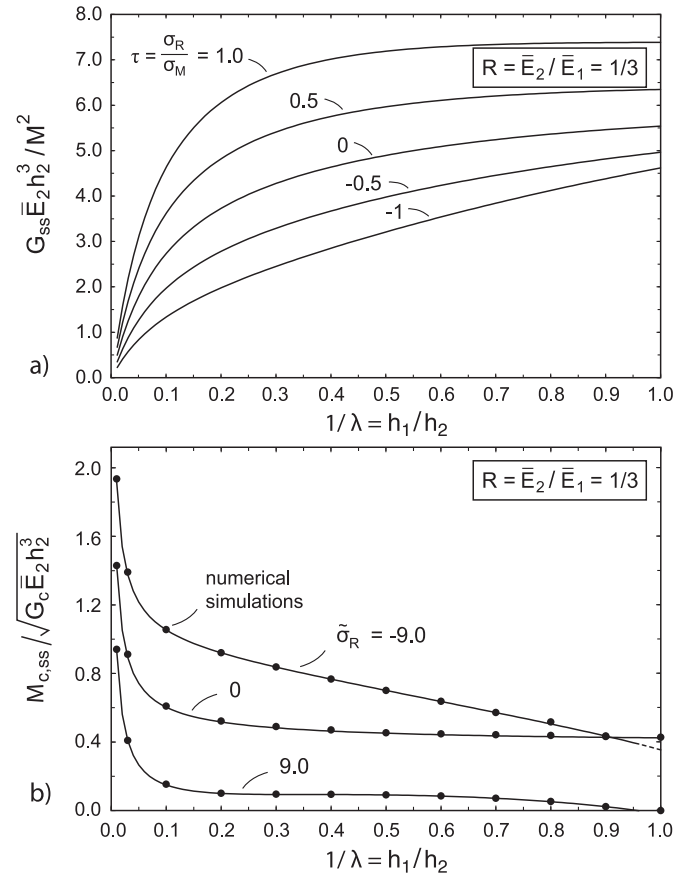


Fig. 8. Elastic film-substrate system: a) Steady-state energy release rate for delamination G_{ss} (in dimensionless form) as a function of the relative film thickness, h_1/h_2 , for different loading parameters, $\tau = \sigma_R/\sigma_M$. b) Critical bending moment for steady-state delamination $M_{c,ss}$ (in dimensionless form), as a function of the relative film thickness, h_1/h_2 , for three different values of the (dimensionless) residual stress, $\bar{\sigma}_R = \sigma_R\sqrt{h_2}/(\bar{E}_2G_c) = -9.0, 0, 9.0$ (FEM results are indicated by black dots).

five different values of τ , where a positive sign and a negative sign of τ respectively refer to a tensile and a compressive film residual stress. In the analysis the film is chosen three times stiffer than the substrate, $\bar{E}_2/\bar{E}_1 = 1/3$. With respect to the case where the residual stress is zero ($\tau = 0$), in the considered range of relative film thicknesses a tensile residual stress ($\tau = 0.5$ and $\tau = 1$) increases the energy release rate, while a compressive residual stress ($\tau = -0.5$ and $\tau = -1$) leads to a decrease in the energy release rate. Note that the results obtained are valid only if frictional effects during crack surface contact have a minor influence on the overall failure response, and the film compressive stress remains well below the critical stress for buckling.

4.1.3. Critical bending moment and comparison to FEM

In Fig. 8b the analytical results for steady-state delamination are compared against numerical results obtained with FEM modelling (indicated by black dots), with the delamination simulated by the mixed-mode interface damage model presented in Cid Alfaro et al. (2009), see Section 3 for more details. The analytical results were obtained by assuming brittle interface delamination, in accordance with Griffith's criterion

$$G_{ss} = G_c, \quad (26)$$

where G_c represents the toughness at steady-state delamination, measured at the appropriate mode-mixity. For ideally brittle delamination along the interface of a bimaterial, the mode-mixity typically is defined as the ratio between the shear traction (mode

II) and the normal traction (mode I) measured at an arbitrary, but specified, reference length ahead of the crack tip [Hutchinson and Suo \(1992\)](#); [Rice \(1988\)](#). Alternatively, when simulating delamination with the interface damage model described in [Section 3.1](#), the effect of the mode-mixity is incorporated through a parameter β , which, as indicated by [Eq. \(17\)](#), depends on a combination of the shear and normal displacements measured in the considered material point of the delamination process zone. The actual definition of the mode-mixity, however, does not influence the computational results discussed in this communication, since these are presented by means of dimensionless parameters that explicitly incorporate the effect of the fracture toughness G_c at the appropriate mode-mixity, see, e.g., the definition of the dimensionless critical bending moment depicted on the vertical axis of [Fig. 8b](#). In other words, the presentation of the results for steady-state delamination is *independent* of the toughness value and mode-mixity formulation adopted in the simulations, thereby supporting a broad practical application.

It is further noted that, for reasons of simplicity, the numerical simulations of the four-point bending test do not consider a (possible) variation of the toughness caused by the change in mode-mixity during crack nucleation; the incorporation of this effect would only have a minor influence on the computational results, since steady-state delamination at constant mode-mixity, as reflected by [Eq. \(26\)](#), is already reached when the delamination length becomes larger than a few times the film thickness. In line with the argumentation given above, after reaching a constant mode-mixity the (dimensionless) failure response becomes *independent* of the specific mode I and mode II toughness values, $G_{I,c}$ and $G_{II,c}$, adopted in the numerical simulations, see [Eq. \(18\)](#).

Substituting the sum of the energy release rate components presented in [Eq. \(25\)](#) into [Eq. \(26\)](#) leads to a quadratic expression in terms of the critical bending moment $M_{c,ss}$, for which only the positive root has a physical meaning (since $M_{c,ss}$ must be positive for generating film delamination in a four-point bending test). From the individual components of the energy release rate, [Eq. \(23\)](#), and Griffith's criterion, [Eq. \(26\)](#), it can be concluded that the dimensionless form of the critical bending moment can be uniquely expressed as a function f of only three dimensionless parameters:

$$\frac{M_{c,ss}}{\sqrt{G_c \bar{E}_2 h_2^3}} = f\left(\frac{\bar{E}_2}{\bar{E}_1}, \frac{h_2}{h_1}, \tilde{\sigma}_R\right) \quad \text{with} \quad \tilde{\sigma}_R = \sigma_R \sqrt{\frac{h_2}{\bar{E}_2 G_c}}, \quad (27)$$

where $\tilde{\sigma}_R$ is the dimensionless residual stress. Using the dimensionless form, [Eq. \(27\)](#), the steady-state failure load $M_{c,ss}$ is computed for three different cases, namely for a compressive residual stress, $\tilde{\sigma}_R = -9.0$, a zero residual stress, $\tilde{\sigma}_R = 0$, and a tensile residual stress, $\tilde{\sigma}_R = 9.0$, see [Fig. 8b](#). Further, the stiffness mismatch between the film and substrate is chosen as $R = \bar{E}_2/\bar{E}_1 = 1/3$. The magnitude of the dimensionless residual stress is representative of a broad range of industrial film-substrate systems; for example, it reflects a metallic film with a Young's modulus of 210 GPa and a Poisson's ratio of 0.3 that experiences a residual stress of 50 MPa after deposition on a substrate of 5 mm thickness, whereby the interfacial toughness equals $G_c = 2 \text{ J/m}^2$. The parameters adopted for the interface damage model used in the FEM analyses are listed in [Table 1](#). The small value chosen for the relaxation parameter η_d ensures that the delamination behaviour closely approaches the limit of a *rate-independent* response, $\eta_d \rightarrow 0$. Furthermore, the material length scale for delamination, $v^u \approx 2G_c/t^u$ (= the ultimate separation in the interface damage model), is taken at least one order of magnitude lower than the smallest geometrical length scale in the FEM model (i.e., the film thickness), in order to ensure that the delamination response closely approaches an ideally brittle behaviour. Indeed, [Fig. 8b](#) shows that the analytical and numerical simulations are in excellent agreement for the three residual

Table 1
Material properties for interface damage model.

Parameter	Value
Elastic interfacial stiffness	$K = 1 \times 10^7 \text{ [N/mm}^3\text{]}$
Ultimate normal traction	$t_1^u = 6 \text{ [N/mm}^2\text{]}$
Ultimate shear traction	$t_2^u = 6 \text{ [N/mm}^2\text{]}$
Fracture toughness	$G_{I,c} = G_{II,c} = 2 \text{ [J/m}^2\text{]}$
Relaxation parameter	$\eta_d = 1 \times 10^{-6} \text{ [s]}$

stresses considered. It can be observed that a tensile (compressive) residual stress in the film predominantly decreases (increases) the resistance against steady-state delamination. For relatively large film thicknesses, $0.9 < h_1/h_2 < 1.0$, however, the presence of a compressive stress leads to a steady-state failure load that is *lower* than the failure load for the case of zero residual stress. This is, since for a compressive residual stress the component $G_{RM,ss}$ generally obtains a negative value and $G_{R,ss}$ obtains a positive value, see [Eq. \(23\)](#)_{2,3}, where the net contribution of $G_{R,ss} + G_{RM,ss}$ to the total delamination driving force G_{ss} is *positive* in the range $0.9 < h_1/h_2 < 1.0$, while in the range $h_1/h_2 < 0.9$ it is *negative*. For $h_1/h_2 = 0.9$ the magnitude of both terms is equal, leading to a zero net contribution of the residual stress to the delamination driving force.

4.1.4. Critical residual stress for spontaneous delamination

Observe from [Fig. 8b](#) that for a tensile residual stress of $\tilde{\sigma}_R = 9.0$ the curve intersects with the horizontal axis at $h_1/h_2 = 0.96$, indicating that film-substrate systems with thicker films will not steadily delaminate at this residual stress; in fact, these films delaminate spontaneously due to the presence of the residual stress only, see also [Beuth and Narayan \(1996\)](#); [Wei and Hutchinson \(1997\)](#). A general, closed-form expression for the critical residual stress $\sigma_{R,c}$ for spontaneous delamination can be derived as

$$\begin{aligned} \sigma_{R,c} &= \pm \sqrt{\frac{\xi}{\bar{E}_2 h_2 (\bar{E}_1 h_1^3 + \bar{E}_2 h_2^3)}} \frac{2\bar{E}_1 G_c}{h_1} \\ &= \pm \sqrt{\frac{3R\lambda(1+\lambda)^2 + (1+R\lambda)(1+R\lambda^3)}{R\lambda(1+R\lambda^3)}} \frac{2\bar{E}_1 G_c}{h_1}, \end{aligned} \quad (28)$$

or, in dimensionless form,

$$\tilde{\sigma}_{R,c} = \sigma_{R,c} \sqrt{\frac{h_2}{\bar{E}_2 G_c}} = \pm \sqrt{\frac{6R\lambda(1+\lambda)^2 + 2(1+R\lambda)(1+R\lambda^3)}{R^2(1+R\lambda^3)}}, \quad (29)$$

with the parameter ξ in [Eq. \(28\)](#) given by [Eq. \(4\)](#). The above expression follows from prescribing the external couple in the expression for the energy release rate, [Eq. \(3\)](#), (or its alternative form given by [Eqs. \(22\) and \(23\)](#)) to be zero, $M = 0$, and combining the result with [Eqs. \(22\) and \(26\)](#), followed by solving for the residual stress σ_R . Note that the condition $M = 0$ leaves [Eq. \(23\)](#)₂ as the only non-zero-term in this expression. [Eqs. \(28\) and \(29\)](#) show that the sign of the critical residual stress can be both positive and negative. As indicated by the short dashed line in [Fig. 8b](#), spontaneous delamination by the negative residual stress $\tilde{\sigma}_R = -9.0$ can be prevented for $h_1/h_2 > 0.96$ only if the effect of this compressive residual stress is opposed through *simultaneously* applying (part of) the bending moment M . However, if the compressive residual stress $\tilde{\sigma}_R = -9.0$ fully develops *before* the bending moment is applied, spontaneous delamination occurs for $h_1/h_2 > 0.96$, which is confirmed by the FEM simulations. In [Fig. 9](#) the dimensionless critical residual stress given by [Eq. \(29\)](#) is plotted as a function of the relative film thickness, h_1/h_2 , for various stiffness ratios, $R = \bar{E}_2/\bar{E}_1$. Observe that the critical residual stress for spontaneous delamination (substantially) increases when the (relative) film thickness becomes smaller, or when the (relative) film stiffness increases. It can be further noticed that for a stiffness ratio $R = 0.3$ the value of

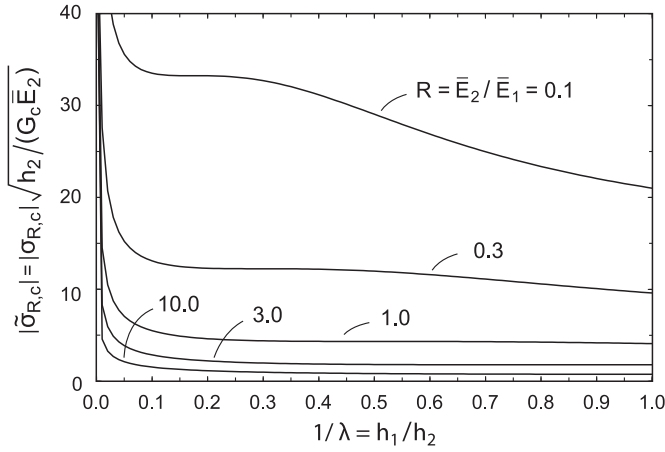


Fig. 9. Absolute value of the critical (dimensionless) residual stress $\bar{\sigma}_{R,c}$ for spontaneous delamination as a function of the relative film thickness, h_1/h_2 , for various stiffness ratios, $R = \bar{E}_2/\bar{E}_1$.

$\bar{\sigma}_{R,c}$ is slightly below 10 when the relative film thickness h_1/h_2 approaches unity, which is in good correspondence with the value $\bar{\sigma}_{R,c} = 9.0$ that appears in Fig. 8b for $R = 1/3$ at a relative film thickness of $h_1/h_2 = 0.96$.

4.1.5. Comparison with other analytical expressions in the literature

The expression for the steady-state energy release rate, Eq. (3) (or its alternative form given by Eqs. (22) and (23)) can be compared to other expressions presented in the literature. A comparison with Eq. (11) presented in Charalambides et al. (1990) which is Ref.[4] in the references listed at the end of this communication, illustrates that the expressions given for the components $G_{M,ss}$ and $G_{RM,ss}$ are identical to those presented by Eqs. (23)₁ and (23)₃. Conversely, the component $G_{R,ss}$ given by Eq. (11) in Charalambides et al. (1990) appears to be different from Eq. (23)₂. This difference can be expressed as

$$\frac{G_{R,ss}(\text{Eq.(11) in Ref.[4]})}{G_{R,ss}(\text{Eq.(23)}_2)} = \frac{3\lambda(1+\lambda)}{(1+R\lambda^3)} + \frac{(1+R\lambda)}{R(1+\lambda)} - \frac{3R\lambda(1+\lambda)^2}{(1+R\lambda^3)(1+R\lambda)}, \quad (30)$$

which vanishes only if the stiffness values of the film and substrate are equal, i.e., for $R = \bar{E}_2/\bar{E}_1 = 1$. Based on the excellent agreement between the present analytical results and FEM results, see Fig. 8b, it is concluded that Eq. (23)₂ is correct, and that the expression for $G_{R,ss}$ given by Eq. (11) in Charalambides et al. (1990) therefore contains errors. The graphical representation of $G_{R,ss}$ in Fig. 11 of Charalambides et al. (1990), however, appears to be correct, and is in full agreement with the representation in Fig. 7b. Hence, it is concluded that the (correct) graphical representation of $G_{R,ss}$ shown in Fig. 11 of Charalambides et al. (1990) is inconsistent with the corresponding (incorrect) closed-form expression given by Eq. (11).

More recently, in Delette et al. (2009), which is Ref.[10] in the references listed at the end of this communication, an alternative closed-form expression was constructed for the steady-state energy release rate of a delaminating film containing a residual stress. The components $G_{M,ss}$ and $G_{R,ss}$ given by Eqs. (23)₁ and (23)₂ are identical to those presented in Eqs. (35) and (36) of Delette et al. (2009). However, the coupling term $G_{RM,ss}$ differs by a factor $\lambda = h_2/h_1$, i.e.,

$$\frac{G_{R,ss}(\text{Eq.(11) in Ref.[10]})}{G_{R,ss}(\text{Eq.(23)}_2)} = \lambda. \quad (31)$$

Obviously, this difference vanishes only if the film and substrate have the same height, for which $\lambda = 1$. Supported by the excellent

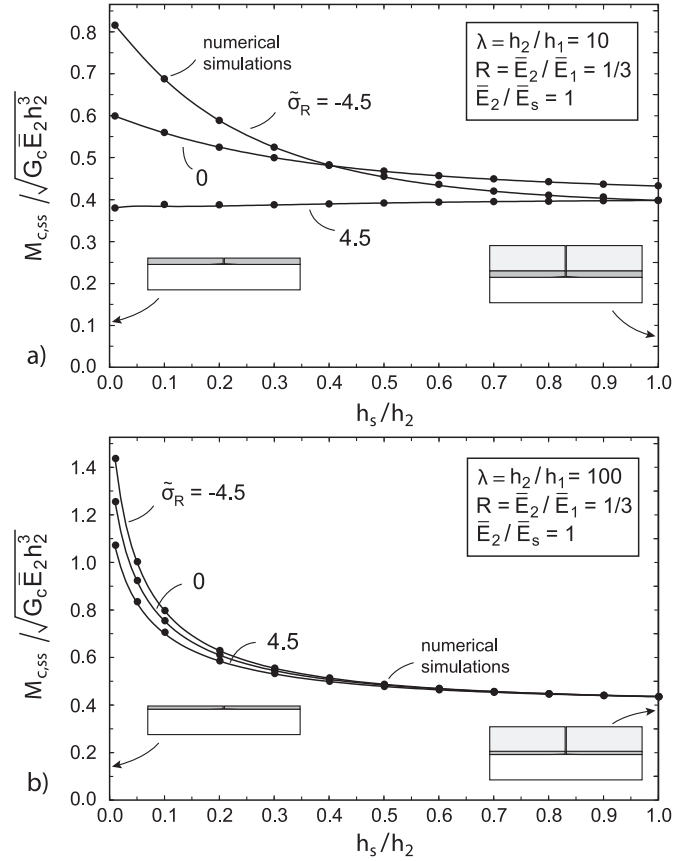


Fig. 10. Elastic film-substrate system with superlayer: Critical bending moment for steady-state delamination $M_{c,ss}$ (in dimensionless form), as a function of the relative thickness of the superlayer, h_s/h_2 , for three different values of the (dimensionless) residual stress, $\bar{\sigma}_R = \sigma_R \sqrt{h_2/(\bar{E}_2 G_c)} = -4.5, 0, 4.5$. The insets show the geometries of the two typical cases $h_s/h_2 = 0$ (superlayer absent) and $h_s/h_2 = 1$ (superlayer and substrate have equal thickness). FEM results are indicated by black dots. a) Layer thickness ratio $\lambda = h_2/h_1 = 10$. b) Layer thickness ratio $\lambda = h_2/h_1 = 100$.

agreement between the results of the current analytical model and the FEM results, see Fig. 8b, it is concluded that the expression for $G_{RM,ss}$ given by Eq. (23)₃ is correct.

4.2. Elastic film-substrate system with additional superlayer

Consider now an elastic film-substrate system extended with an additional superlayer of thickness h_s , Young's modulus E_s and Poisson's ratio ν_s , see Fig. 3. The resistance against steady-state delamination failure is examined for two different thickness ratios, namely $\lambda = h_2/h_1 = 10$ and 100. The film and substrate are further characterised by a relative stiffness $R = \bar{E}_2/\bar{E}_1 = 1/3$, while the stiffness values of the superlayer and the substrate are taken equal, $\bar{E}_s/\bar{E}_2 = 1$. The dimensionless values of the residual stress in the film are chosen the same as for the basic film-substrate system analysed in Section 4.1.2, i.e., $\bar{\sigma}_R = \sigma_R \sqrt{h_2/(\bar{E}_2 G_c)} = -4.5, 0$ and 4.5.

4.2.1. Critical bending moment and comparison to FEM

The delamination resistance is examined by plotting the critical moment for steady-state delamination, $M_{c,ss}$ as a function of the relative thickness h_s/h_2 of the superlayer, see Fig. 10. Here, the delamination resistance for a film-substrate system without a superlayer is retrieved at $h_s/h_2 = 0$, and the system of a film sandwiched between two identical layers (see also Section 2.2.1) is obtained at $h_s/h_2 = 1$. These two configurations are visualised in the insets of Fig. 10. It can be noticed that the FEM results (black dots)

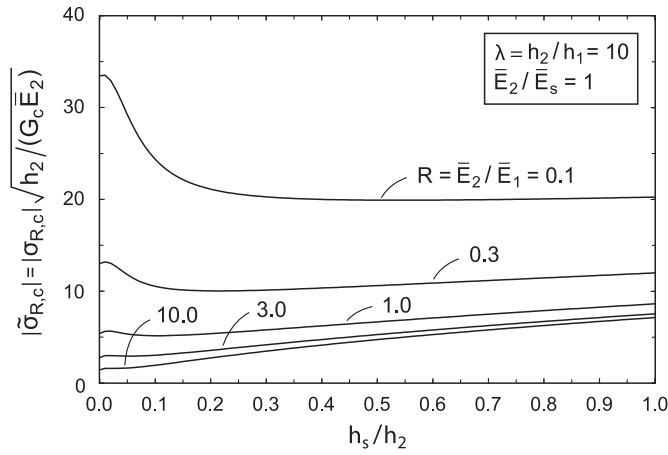


Fig. 11. Absolute value of the critical (dimensionless) residual stress $\bar{\sigma}_{R,c}$ for spontaneous delamination as a function of the relative thickness of the superlayer, h_s/h_2 , for various stiffness ratios, $R = \bar{E}_2/\bar{E}_1$.

are in excellent agreement with the analytical results (solid lines) computed with the closed-form expression, Eq. (6).

The effect of the superlayer in almost all cases manifests itself through a decreasing value of the critical bending moment $M_{c,ss}$ for an increasing thickness h_s of the superlayer, as caused by an increasing delamination driving force G_{ss} . This illustrates the efficiency of the superlayer in bringing down the failure load required for steady-state interfacial delamination, such that in a four-point bending test it may end up lower than the failure load of an alternative, undesirable fracture mode. An exception to this trend can be observed for the case of a tensile residual stress $\bar{\sigma}_R = 4.5$ plotted in Fig. 10a, for which the critical bending moment for delamination is nearly unaffected by the thickness h_s of the superlayer. In other words, the addition of a superlayer here does not increase the driving force for interfacial delamination. In comparison to the configuration where the residual stress is absent, $\bar{\sigma}_R = 0$, the presence of a compressive stress $\bar{\sigma}_R = -4.5$ leads to higher critical bending moment only if the relative thickness of the superlayer is relatively small, in the range of $0 < h_s/h_2 < 0.4$. The crossing of the two curves at $h_s/h_2 = 0.4$ is comparable to the crossing of curves at $h_1/h_2 = 0.9$ for the film-substrate system without a superlayer, see Fig. 8b, and thus follows a similar explanation as provided in Section 4.1.3.

Comparing the curves for $\lambda = h_2/h_1 = 10$ in Fig. 10a with those for the thinner film $\lambda = h_2/h_1 = 100$ depicted in Fig. 10b, it can be concluded that a thinner film typically benefits more from the addition of a superlayer, by showing a higher decrease in the critical bending moment for delamination failure under increasing thickness of the superlayer. Furthermore, the effect of the residual stress on the driving force for interfacial delamination clearly diminishes for thicker superlayers; for the case $\lambda = h_2/h_1 = 100$ this effect even virtually vanishes for $h_s/h_2 > 0.5$. Moreover, both for $\lambda = h_2/h_1 = 10$ and $\lambda = 100$ the curves for a tensile and compressive residual stress intersect at $h_s/h_2 = 1$; this is due to the symmetry of this configuration, causing the coupling term in the energy release rate to vanish, $G_{RM,ss} = 0$. Consequently, the total driving force for delamination becomes independent of the sign of the residual stress, see also Eq. (9).

4.2.2. Critical residual stress for spontaneous delamination

The critical residual stress required for generating spontaneous delamination can be straightforwardly computed by equating the bending moment in Eq. (6) to zero, $M = 0$, substituting the result in Griffith's criterion, Eq. (26), and solving for σ_R . This leads to

$$\sigma_{R,c} = \pm \left[\left(\frac{-3\bar{E}_1 h_1 (\bar{E}_2 h_2 - \bar{E}_s h_s) + \bar{E}_2 h_2^2 - \bar{E}_s h_s^2}{(\bar{E}_1 h_1 + \bar{E}_2 h_2 + \bar{E}_s h_s) \gamma} + \gamma \right) \left(\frac{\bar{E}_s h_s (\bar{E}_1 h_1^3 + \bar{E}_s h_s^3)}{\beta} \right)^{-1} \frac{2\bar{E}_1 G_c}{h_1} \right]^{1/2}, \quad (32)$$

with the parameters β and γ given by Eq. (7). In the absence of a superlayer, $h_s/h_2 = 0$, Eq. (32) reduces to the expression for the critical stress for spontaneous delamination in the basic film-substrate system, Eq. (28). In Fig. 11 the critical residual stress given by Eq. (32) is plotted in dimensionless form as a function of the relative thickness of the superlayer, h_s/h_2 , for various stiffness ratios, $R = \bar{E}_2/\bar{E}_1$. Here, the film thickness is taken ten times smaller than the substrate thickness, $h_2/h_1 = 10$, and the stiffness values of the superlayer and the substrate are assumed to be equal, $\bar{E}_2/\bar{E}_s = 1$. For relatively stiff films ($R < 1$) the critical residual stress initially drops at increasing thickness h_s of the superlayer, but for larger thickness starts to slightly increase. For relatively flexible films ($R > 1$), however, the critical residual stress for spontaneous delamination monotonically increases at increasing thickness of the superlayer. This trend is in agreement with the observation from Fig. 9 that the resistance against spontaneous delamination decreases when the relative film thickness (which here equals $h_1/(h_2 + h_s)$) becomes smaller. Note further that at $h_s/h_2 = 0$ (superlayer is absent) the values of $\bar{\sigma}_{R,c}$ correspond to those plotted in Fig. 9 at a relative film thickness $\lambda^{-1} = h_1/h_2 = 0.1$.

4.3. Elastic film supported by an elasto-plastic substrate

Consider now the configuration of an elastic film supported by an elasto-plastic substrate, see also Fig. 4. In the spirit of Wei and Hutchinson (1997), by means of a dimensional analysis the critical bending moment $M_{c,ss}$ for steady-state delamination of the film can be expressed as a function of the following eight dimensionless parameters:

$$\frac{M_{c,ss}}{\sqrt{G_c \bar{E}_2 h_2^3}} = f \left(\frac{\bar{E}_2}{\bar{E}_1}, \frac{h_2}{h_1}, \bar{\sigma}_R, \frac{h_2}{R_0}, \frac{t^u}{\sigma_y}, \alpha, N, \frac{E_2}{\sigma_y} \right), \quad (33)$$

where, in correspondence with the elastic systems considered previously, the Poisson's ratios of the film and substrate are taken as: $\nu_1 = \nu_2 = 0.3$. The dimensionless residual stress $\bar{\sigma}_R$ is presented in Eq. (27). When comparing Eq. (33) with the dimensionless form for the elastic film-substrate system, Eq. (27), it is clear that the difference becomes manifest through the last five, plasticity-related parameters in the function f . In the parameter variation study presented below, four of the eight dimensionless parameters are kept fixed, i.e., the stiffness mismatch equals $R = \bar{E}_2/\bar{E}_1 = 1/3$, and the material parameters of the Ramberg–Osgood model, Eq. (12), are $\alpha = 3/7$, $N = 5$ and $E_2/\sigma_y = 580$.

4.3.1. Critical bending moment

Fig. 12 shows the critical bending moment $M_{c,ss}$ versus the relative film thickness $\lambda^{-1} = h_1/h_2$ for four different values of the relative strength of the material interface, $t^u/\sigma_y = 0.05, 0.5, 1.0$ and 2.0 . Furthermore, the (semi-)analytical solutions for an elastic substrate and an elasto-plastic substrate (where $t^u/\sigma_y = 0$) are depicted for comparison. In Fig. 12a the length scale parameter related to the size of the plastic zone equals $h_2/R_0 = 27.5$, while in Fig. 12b it is set ten times higher, $h_2/R_0 = 275$. First the delamination resistance under pure bending is analysed, by leaving out the effect of the residual stress, $\bar{\sigma}_R = 0$. It can be observed that the overall delamination resistance varies strongly in the range of small film thicknesses, $h_1/h_2 < 0.5$, but starts to level off for larger film thicknesses. In the limit of zero delamination strength,

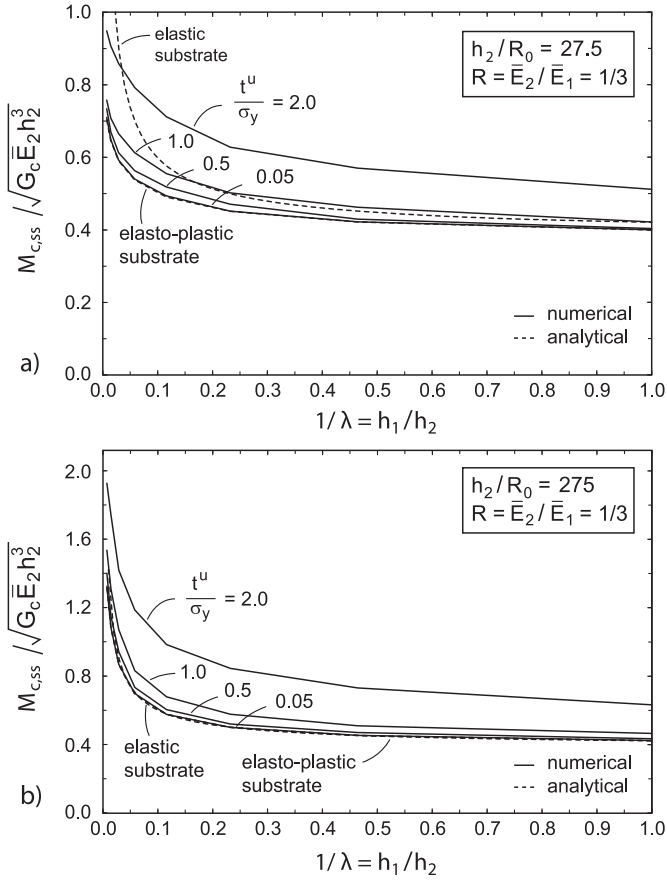


Fig. 12. Elasto-plastic film-substrate system: Critical bending moment for steady-state delamination $M_{c,ss}$ (in dimensionless form) as a function of the relative film thickness, h_1/h_2 , for four different values of the relative interfacial strength, $t^u/\sigma_y = 0.05, 0.5, 1.0, 2.0$ (solid lines). The (semi-)analytical solutions for the film on an elastic substrate and on elasto-plastic substrate (for which $t^u/\sigma_y = 0.0$) are plotted for comparison (dashed lines). a) Relatively large plastic zone, $h_2/R_0 = 27.5$. b) Relatively small plastic zone, $h_2/R_0 = 275$.

$t^u/\sigma_y \rightarrow 0$, the FEM results in Fig. 12a and b converge towards the corresponding semi-analytical solution treated in Section 2.3. As mentioned before, the semi-analytical solution only takes into account bulk plasticity at the downstream and upstream cross-sections, and ignores local plasticity near the delamination tip. For an increasing relative interfacial strength t^u/σ_y , however, the plastic dissipation at the delamination tip starts to grow, as a result of which the effective resistance against delamination increases and the failure curves start to deviate from the semi-analytical solution obtained for $t^u/\sigma_y = 0$.

It is interesting to notice that for a relatively small plastic zone, $h_2/R_0 = 275$, the analytical solutions for the elastic and the elasto-plastic film-substrate systems are virtually identical over almost the complete range of values h_1/h_2 considered in Fig. 12b. This indeed indicates that the amount of plastic dissipation is negligible compared to the dissipation generated by interfacial delamination, and that the *small scale yielding* condition is satisfied. Moreover, the analytical solution for the elastic system (given by Eq. (3)) leads to a reasonable approximation for the delamination resistance of the elasto-plastic film-substrate system in the case of low relative interfacial strengths, $0 < t^u/\sigma_y \leq 0.5$. For a ten times larger plastic zone, $h_2/R_0 = 27.5$, this approximation is reasonable for relatively large film thicknesses, but becomes inaccurate when the film is sufficiently thin to develop *large scale yielding*, say when $h_1/h_2 < 0.5$, see Fig. 12a. For a low relative interfacial strength the elastic solution then *overpredicts* the critical bending moment

$M_{c,ss}$. This is, since the stiffness reduction at the downstream cross-section caused by plasticity increases the drop in strain energy from the upstream to the downstream cross-section, and thereby the driving force for delamination. Accordingly, the critical bending moment for delamination is lower than for the elastic film-substrate system. Large scale yielding here is mainly characterised by bulk plasticity generated at the downstream cross-section, since the substrate stress at the delamination tip is kept small by the low interfacial strength value t^u , and therefore does not reach the yield strength. Conversely, as illustrated by the case $t^u/\sigma_y = 2$, at high relative interfacial strength the elastic solution for most values of h_1/h_2 typically *underpredicts* the critical bending moment. The resistance against delamination now is also dictated by the relatively high critical stress t^u at the delamination tip, where stress relaxations induced by large scale yielding make it more difficult to reach this strength value, thus requiring the application of a higher critical bending moment (i.e., more external work) than for the elastic system. In summary, with reference to the elastic solution, large scale yielding may *decrease* or *increase* the critical bending moment $M_{c,ss}$, depending on whether the resistance against delamination is determined *mildly* (low values of t^u/σ_y) or *strongly* (high values of t^u/σ_y) by the relative interfacial strength, respectively.

In the limit of an infinitesimal film thickness, $h_1/h_2 \rightarrow 0$, the elastic energy available for delamination goes to zero, i.e., the upstream energy then becomes equal to the downstream energy. Consequently, the critical bending moment $M_{c,ss}$ for the elastic film-substrate system becomes infinitely large. In contrast, the critical bending moment for the elasto-plastic film-substrate system in this limit remains finite, as the stress generated by bending of the substrate remains finite, and at some state of deformation will meet the strength t^u required for initiating delamination. For this reason, in Fig. 12a the delamination curve for the elasto-plastic system with high interfacial strength, $t^u/\sigma_y = 2$, crosses the curve for the elastic system when the film thickness goes towards zero.

In Fig. 12a the transition from small scale yielding to large scale yielding at moderate to low interfacial strengths, $t^u/\sigma_y \leq 1$, is observed to occur at a relative film thickness of $h_1/R_0 = (h_1/h_2) \times (h_2/R_0) \approx 0.5 \times 27.5 \approx 14$. Here, at values of $h_1/h_2 \geq 0.5$ the relative difference between the critical bending moment for the configurations with the elastic substrate and the elasto-plastic substrate with $t^u/\sigma_y \leq 1$ remains limited to 6% or less. The value of $h_1/R_0 \approx 14$ serves as a rough approximation, and may change if in Eq. (33) the values of the dimensionless parameters for the Ramberg-Osgood plasticity model are chosen differently. The value further depends on the specific geometry and the type of loading conditions applied to the film-substrate system; for example, for an elastic film delaminating from a semi-infinite, elasto-plastic substrate under the presence of a residual stress, the transition from small scale yielding to large scale yielding for a broad range of relative interfacial strengths occurs at a value of $h_1/R_0 \approx 5$, see Fig. 3 in Wei and Hutchinson (1997).

4.3.2. Effect of residual stress on delamination resistance

The combined effect of the externally applied couple M and the residual stress σ_R on the delamination resistance of the film is shown in Fig. 13 for the case of the relatively large plastic zone, $h_2/R_0 = 27.5$, by considering two values of the relative interfacial strength, $t^u/\sigma_y = 0$ (computed with the semi-analytical model treated in Section 2.3) and $t^u/\sigma_y = 2$ (computed with FEM). The delamination resistance is illustrated for three values of the dimensionless residual stress, namely a tensile residual stress $\bar{\sigma}_R = 4.5$, zero residual stress $\bar{\sigma}_R = 0$, and a compressive residual stress $\bar{\sigma}_R = -4.5$. The results for the case $\bar{\sigma}_R = 0$ are in accordance with those plotted in Fig. 12a. It can be observed that the effect of the

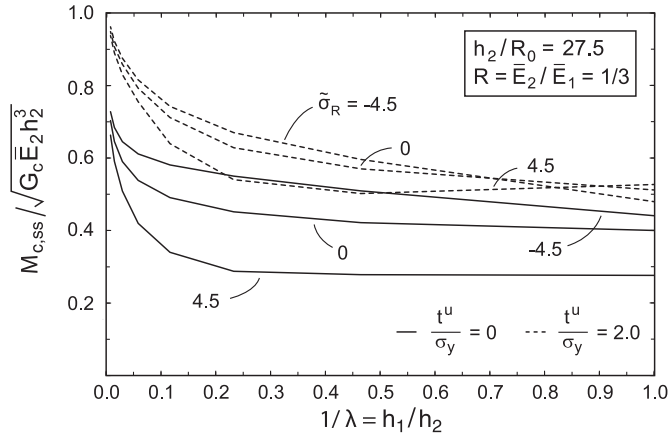


Fig. 13. Elasto-plastic film-substrate system: Critical bending moment for steady-state delamination $M_{c,ss}$ (in dimensionless form) as a function of the relative film thickness, h_1/h_2 , for three different values of the (dimensionless) residual stress, $\bar{\sigma}_R = \sigma_R \sqrt{h_2 / (\bar{E}_2 G_c)} = -4.5, 0, 4.5$, at two values of the relative interfacial strength, $t^u/\sigma_y = 0$ (solid lines) and 2.0 (dashed lines). The size of the plastic zone is relatively large, in correspondence with $h_2/R_0 = 27.5$.

residual stress on the delamination resistance to a large extent is comparable to that of the elastic film-substrate system depicted in Fig. 8b, in a sense that compressive and tensile residual stresses mostly lead to an increase and decrease of the delamination resistance, respectively. Nevertheless, at the interfacial strength of $t^u/\sigma_y = 2$ this trend reverses when the film thickness becomes relatively large, i.e., when $h_1/h_2 > 0.8$. This can be ascribed to the fact that for a tensile residual stress the von Mises equivalent plastic strain at the delamination tip increases when the relative film thickness increases from $h_1/h_2 = 0.5$ to 1.0 , thereby increasing the overall delamination resistance, while for a compressive residual stress it then decreases. Correspondingly, under the tensile residual stress the substrate with a high interfacial strength, $t^u/\sigma_y = 2$, experiences large scale yielding over the whole range of considered film thicknesses, $0 < h_1/h_2 \leq 1.0$. Conversely, under the compressive residual stress the limit of small scale yielding is approached at $h_1/h_2 = 1.0$, as can be confirmed from the rather close agreement between the value of the corresponding critical bending moment and that for the case of zero interfacial strength, $t^u/\sigma_y = 0$. In other words, for the compressive residual stress the critical bending moment at $h_1/h_2 = 1.0$ becomes almost insensitive to the value of the relative interfacial strength, and then essentially is determined by the fracture toughness G_c .

Note that for the case of a high relative interfacial strength, $t^u/\sigma_y = 2$, the notion of small scale yielding requires that *both* at the delamination tip and at the downstream (and, to a lesser extent, upstream) cross-section(s) of the substrate the size of the plastic zone R_0 remains significantly smaller than any of the geometrical length scales (i.e., film thickness, substrate thickness). This is different for the case of a moderate to low relative interfacial strength, $t^u/\sigma_y < 1$, where the notion of small scale yielding only imposes restrictions to the size of the plastic zone at the downstream and upstream cross-sections, as the stress at the delamination tip then unconditionally remains in the elastic range.

Comparing the curves for $t^u/\sigma_y = 0$ with those for $t^u/\sigma_y = 2$ shows that the effect of the residual stress on the delamination resistance decreases for a higher relative strength of the material interface. This is due to the fact that a film-substrate system with a higher interfacial strength requires a higher critical bending moment $M_{c,ss}$ for generating delamination failure, as a result of which the relative contribution of the actual residual stress to the driv-

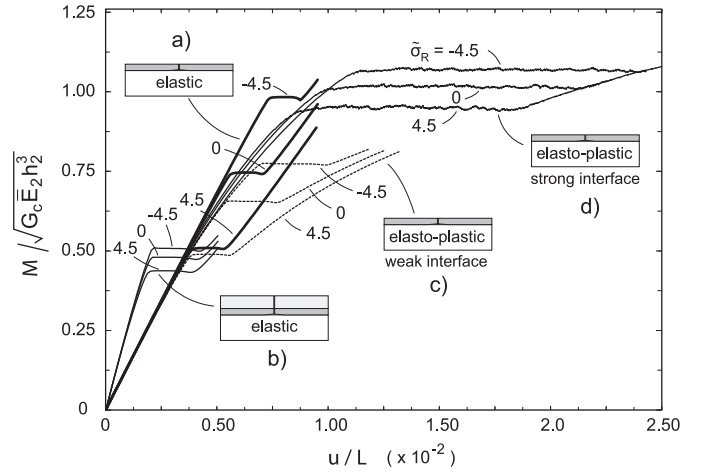


Fig. 14. Delamination response of film-substrate systems subjected to four-point bending, for three different values of the (dimensionless) residual stress in the film, $\bar{\sigma}_R = \sigma_R \sqrt{h_2 / (\bar{E}_2 G_c)} = -4.5, 0, 4.5$. a) Elastic system. b) Elastic system with a superlayer added. c) Elasto-plastic system with relatively weak interface ($t^u/\sigma_y = 0.2$). d) Elasto-plastic system with relatively strong interface ($t^u/\sigma_y = 2.0$).

ing force for steady-state delamination automatically becomes less. This effect has also been analysed for the elastic film-substrate system through the loading parameter τ given by Eq. (24), where a higher bending moment M reduces the value of τ , and thus the relative influence of the residual stress on the driving force for steady-state delamination, see Eq. (25) and Fig. 8a. Obviously, in the limit of $M \rightarrow \infty$ the relative contribution of the residual stress to the delamination driving force vanishes.

4.4. Moment-displacement curves under four-point bending

Fig. 14 illustrates the four-point bend delamination responses of the four film-substrate systems considered in this communication, which are labelled as: a) an elastic film-substrate system, b) an elastic film-substrate system with a superlayer added, c) an elastic film on an elasto-plastic substrate with a weak interface, and d) an elastic film on an elasto-plastic substrate with a strong interface. All responses are computed with FEM, whereby the stiffness mismatch is $R = \bar{E}_2/\bar{E}_1 = 1/3$, and the ratio of layer thicknesses equals $\lambda = h_2/h_1 = 20$. The parameters for the Ramberg-Osgood model are $\alpha = 3/7$, $N = 5$ and $E_2/\sigma_y = 2330$. The stiffness of the superlayer is equal to that of the substrate, $\bar{E}_s/\bar{E}_2 = 1$, and the thickness ratio equals $h_s/h_2 = 0.5$. The weak and strong interfaces have relative strengths of $t^u/\sigma_y = 0.2$ and $t^u/\sigma_y = 2.0$, respectively. The relative size of the plastic zone is taken in accordance with $h_2/R_0 = 70$, and the three values of the dimensionless residual stress are $\bar{\sigma}_R = 4.5, 0$ and -4.5 . Note that some of the parameters above have a different value than used for the studies in Sections 4.1 and 4.3, which was done for optimizing the graphical representation in Fig. 14. The vertical displacement u , depicted on the horizontal axis in dimensionless form, refers to the point of load application, located at distance L from the inner loading line of the specimen. Note that all moment-displacement curves are characterised by a horizontal plateau, indicating the occurrence of steady-state delamination. For an elasto-plastic substrate the length of this plateau is longer than for an elastic substrate, as part of the vertical displacement u is due to plastic dissipation. The process of steady-state delamination is abandoned when the delamination tip approaches the inner loading point, and the resistance against delamination starts to increase due to crack face contact. For an elastic substrate the tangent (stiffness) correspond-

ing to this rising part of the curve obviously is larger than for an elasto-plastic substrate.

In the FEM simulations with the elasto-plastic substrate, the size of the film thickness only is a few times the size of the plastic zone, i.e., $h_1/R_0 = 3.5$. This ratio is smaller than the value $h_1/R_0 \approx 14$ characterizing the global transition from small scale yielding to large scale yielding, see Section 4.3.2, thus indicating that large scale yielding occurs. As explained in Section 4.3.2, it can be indeed observed that for an elasto-plastic substrate with a weak interface the delamination resistance is lower than for an elastic substrate, while for an elasto-plastic substrate with a strong interface it is higher. Furthermore, stress relaxation induced by large scale yielding clearly decreases the effect by the residual stress on the delamination resistance. For the elastic film-substrate system the addition of a superlayer also decreases the effect by the residual stress. Moreover, it substantially reduces the critical moment for steady-state delamination, due to an increase of the delamination driving force G_{SS} .

5. Concluding remarks

The analytical models and numerical results presented in this communication may serve as a useful tool in the design against thin film delamination, and may support the experimental determination of the delamination toughness of thin films experiencing residual stresses. To further investigate these effects, more systematic experimental studies are necessary, both on elastic and elasto-plastic film-substrate systems. It is thereby important to accurately measure the evolution of the residual stress in the film during film deposition or temperature excursion, using mechanical methods, capacitance methods, X-ray diffraction methods or optical methods, see Freund and Suresh (2003). The sensitivity of the current results to material anisotropy and geometric inhomogeneities (microstructural defects, non-uniform film thickness, film patterning, etc.) are also topics for future studies, as well as a systematic analysis of the effect of film plasticity on the resistance against delamination.

Appendix A. Steady-state energy release rate of an elastic film delaminating from an elastic substrate under bending and a residual stress

Fig. A.1 shows a film-substrate system in a four-point bend testing set-up, with a delaminating crack evolving along the interface between the film and the substrate. The delaminating crack is driven by a couple M and a uniform residual stress σ_R (where a positive sign denotes *tension* and a negative sign denotes *compression*). Whether the curvature is positive (which is in correspondence with the deformed configuration sketched in Fig. A.1) or negative depends on the signs of the moment M and the residual stress σ_R ; a positive bending moment M (which corresponds to the direction of M denoted in Fig. A.1, considering a right-handed coordinate system with the positive y -axis pointing downwardly) and/or a negative residual stress σ_R provide the system with a positive curvature, whereas a negative moment M and/or a positive residual stress σ_R provide the system with a negative curvature. From symmetry in the geometry and the applied loading, only half of the film-substrate system needs to be considered, see Fig. A.1. At the downstream cross-section the neutral axis is located halfway the height h_2 of the substrate. At the upstream cross-section the neutral axis is located at distance a from the bottom of the substrate and at distance b from the top of the substrate. The vertical distance from the neutral line is measured along the y -axis, where the downward direction is taken as positive.

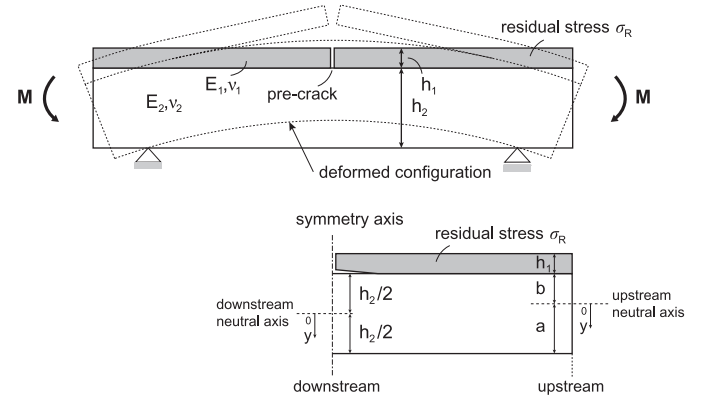


Fig. A.1. Film-substrate system subjected to an external couple M and a residual stress σ_R in the film.

Location of neutral line at upstream cross-section

In accordance with the requirement of force equilibrium, the integral of the “elemental forces” over the entire upstream cross-section needs to be equal to zero,

$$\int_1 \sigma_{u1} dA + \int_2 \sigma_{u2} dA = 0, \quad (A.1)$$

with σ_{u1} and σ_{u2} the normal stresses in the longitudinal direction of the film and the substrate, respectively, and A the upstream cross-section. The constitutive relations for the elastic film and substrate under a state of bending with a residual stress σ_R present in the film are

$$\begin{aligned} \sigma_{u1} &= -\bar{E}_1 \kappa_u y + \sigma_R, \\ \sigma_{u2} &= -\bar{E}_2 \kappa_u y, \end{aligned} \quad (A.2)$$

where \bar{E}_i with $i = 1, 2$ are the plane-strain moduli of the film and substrate, as given by $\bar{E}_i = E_i / (1 - \nu_i^2)$ with E_i the Young's modulus and ν_i the Poisson's ratio. Further, κ_u is the curvature of the upstream cross-section, generated by *both* the couple M and the uniform residual stress σ_R . Substituting Eq. (A.2) into Eq. (A.1) leads to

$$\bar{E}_1 \int_{y=-b-h_1}^{-b} \left(-\kappa_u y + \frac{\sigma_R}{\bar{E}_1} \right) dy + \bar{E}_2 \int_{y=-b}^a -\kappa_u y dy = 0, \quad (A.3)$$

where h_1 is the thickness of the film, and a and b indicate the location of the neutral axis, as shown in Fig. A.1. The curvature κ_u can be expressed in terms of the couple M and the residual stress σ_R through combining Eq. (A.2) with the moment equilibrium. Accordingly, the integral of “elemental moments” over the entire cross-section is equated to the external moment M :

$$-\int_{-b-h_2}^{-b} \sigma_{u1} y dy - \int_{-b}^a \sigma_{u2} y dy = M. \quad (A.4)$$

With the constitutive relations given by Eq. (A.2), this expression turns into

$$-\bar{E}_1 \int_{y=-b-h_1}^{-b} \left(-\kappa_u y + \frac{\sigma_R}{\bar{E}_1} \right) y dy + \bar{E}_2 \int_{y=-b}^a \kappa_u y^2 dy = M. \quad (A.5)$$

Carrying out the integration of Eqs. (A.3) and (A.5), and using the relation $b = h_2 - a$, the upstream curvature κ_u becomes

$$\kappa_u = \frac{12M(\bar{E}_1 h_1 + \bar{E}_2 h_2) - 6\sigma_R h_1 h_2 \bar{E}_2 (h_1 + h_2)}{\xi},$$

$$\text{with } \xi = \bar{E}_1^2 h_1^4 + 4\bar{E}_1 h_1^3 \bar{E}_2 h_2 + 6\bar{E}_1 h_1^2 \bar{E}_2 h_2^2 + 4\bar{E}_1 h_1 \bar{E}_2 h_2^3 + \bar{E}_2^2 h_2^4. \quad (\text{A.6})$$

Further, the expressions for a and b are obtained as

$$a = \frac{6M(\bar{E}_2 h_2^2 + \bar{E}_1 h_1 (h_1 + 2h_2)) + \sigma_R (\bar{E}_1 h_1^4 - \bar{E}_2 h_2^2 h_1 (3h_1 + 2h_2))}{12M(\bar{E}_1 h_1 + \bar{E}_2 h_2) - 6\sigma_R \bar{E}_2 h_1 h_2 (h_1 + h_2)},$$

$$b = \frac{6M(\bar{E}_2 h_2^2 - \bar{E}_1 h_1^2) - \sigma_R (\bar{E}_1 h_1^4 + \bar{E}_2 h_2^2 h_1 (3h_1 + 4h_2))}{12M(\bar{E}_1 h_1 + \bar{E}_2 h_2) - 6\sigma_R \bar{E}_2 h_1 h_2 (h_1 + h_2)}. \quad (\text{A.7})$$

Strain energy upstream and downstream

The upstream strain energy (per unit width) is obtained by integrating the strain energy density over the cross-section:

$$U_u = \frac{1}{2} \bar{E}_1 \int_{y=-b-h_1}^{-b} (-\kappa_u y + \frac{\sigma_R}{\bar{E}_1})^2 dy + \frac{1}{2} \bar{E}_2 \int_{y=-b}^a (-\kappa_u y)^2 dy. \quad (\text{A.8})$$

Inserting Eqs. (A.6) and (A.7) into Eq. (A.8) then results in

$$U_u = \frac{12M^2 \bar{E}_1 (\bar{E}_1 h_1 + \bar{E}_2 h_2) + \sigma_R^2 \bar{E}_2 h_1 h_2 (\bar{E}_1 h_1^3 + \bar{E}_2 h_2^3)}{2\bar{E}_1 \xi}, \quad (\text{A.9})$$

with ξ given in Eq. (A.6). The strain energy at the downstream cross-section is computed in a similar fashion as for the upstream cross-section. Since the downstream cross-section is homogeneous and does not experience the residual stress σ_R (due to the development of delamination), the neutral axis is positioned at a distance $h_2/2$ from the bottom of the substrate, see Fig. A.1. Requiring the integral of elemental moments over the cross-section to be equal to M ,

$$-\int_{y=-h_2/2}^{h_2/2} \sigma_{d2} y dy = M, \quad (\text{A.10})$$

followed by substituting the constitutive equation, $\sigma_{d2} = -\bar{E}_2 \kappa_d y$, and solving for the downstream curvature κ_d , gives

$$\kappa_d = \frac{12M}{\bar{E}_2 h_2^3}. \quad (\text{A.11})$$

Subsequently, the strain energy density is integrated over the downstream cross-section as

$$U_d = \frac{1}{2} \bar{E}_2 \int_{y=-h_2/2}^{h_2/2} (-\kappa_d y)^2 dy, \quad (\text{A.12})$$

which, with Eq. (A.11), results in

$$U_d = \frac{6M^2}{\bar{E}_2 h_2^3}. \quad (\text{A.13})$$

The decrease in strain energy ΔU during delamination over a distance a can be calculated from the difference in the strain energy downstream and upstream as

$$\Delta U = (U_d - U_u)a$$

$$= \left(\frac{6M^2}{\bar{E}_2 h_2^3} - \frac{12M^2 \bar{E}_1 (\bar{E}_1 h_1 + \bar{E}_2 h_2) + \sigma_R^2 \bar{E}_2 h_1 h_2 (\bar{E}_1 h_1^3 + \bar{E}_2 h_2^3)}{2\bar{E}_1 \xi} \right) a, \quad (\text{A.14})$$

where the final result has been obtained by using Eqs. (A.9) and (A.13).

Energy balance and steady-state energy release rate

The steady-state energy release rate for the delaminating crack depicted in Fig. A.1 can be computed from the energy balance

$$\Delta W = \Delta F - \Delta U, \quad (\text{A.15})$$

where ΔW is the interfacial energy consumed during delamination, ΔU is the drop in strain energy as a result of delamination (in accordance with Eq. (A.14)), and ΔF is the external work applied to the film-substrate system. The external work follows from the product of the bending moment M and the energetically-conjugated rotation ϕ . The rotation is determined by the product of the delamination a and the difference in curvature of the downstream and upstream cross-sections, i.e.,

$$\phi = (\kappa_d - \kappa_u)a. \quad (\text{A.16})$$

Substituting Eqs. (A.6) and (A.11) into Eq. (A.16), and using the result in the definition for the external work, leads to

$$\Delta F = M\phi$$

$$= \left(\frac{12M^2}{\bar{E}_2 h_2^3} - \frac{12M^2 (\bar{E}_1 h_1 + \bar{E}_2 h_2) - 6\sigma_R M h_1 h_2 \bar{E}_2 (h_1 + h_2)}{\xi} \right) a. \quad (\text{A.17})$$

Inserting Eqs. (A.14) and (A.17) into Eq. (A.15), the steady-state energy release rate G_{ss} for delamination can be computed from

$$G_{ss} = \frac{\partial \Delta W}{\partial a} = \frac{\partial (\Delta F - \Delta U)}{\partial a}, \quad (\text{A.18})$$

leading to the closed-form expression

$$G_{ss} = 6M^2 \left(\frac{1}{\bar{E}_2 h_2^3} - \frac{(\bar{E}_1 h_1 + \bar{E}_2 h_2)}{\xi} \right) + \frac{\sigma_R^2 \bar{E}_2 h_1 h_2 (\bar{E}_1 h_1^3 + \bar{E}_2 h_2^3) + 12\sigma_R M \bar{E}_1 h_1 \bar{E}_2 h_2 (h_1 + h_2)}{2\bar{E}_1 \xi}, \quad (\text{A.19})$$

with the parameter ξ given by Eq. (A.6). The above expression is used in the analytical study of steady-state delamination, see Eq. (3) in Section 2.

Appendix B. Some expressions from the deformation theory of plasticity

In accordance with the deformation theory of plasticity, the elasto-plastic material response is modelled by means of a non-linear elastic formulation

$$\varepsilon_m = \frac{\sigma_m}{E} + \alpha \frac{\sigma_m}{E} \left(\frac{\sigma_m}{\sigma_y} \right)^{N-1}, \quad (\text{B.1})$$

known as the Ramberg–Osgood model (Ramberg and Osgood, 1943). Here, ε_m and σ_m formally represent the uniaxial strain and stress, respectively, E is Young's modulus, σ_y is the yield strength, and α and N are parameters describing the specific hardening behaviour of the material. This uniaxial constitutive relation can also be used under multiaxial loading conditions, by taking σ_m and ε_m as equivalent stress and strain measures, respectively. The expressions for these equivalent measures commonly are chosen in accordance with a von Mises formulation,

$$\sigma_m = \sqrt{\frac{1}{2} [(\sigma_{xx} - \sigma_{yy})^2 + (\sigma_{yy} - \sigma_{zz})^2 + (\sigma_{zz} - \sigma_{xx})^2] + 3(\sigma_{xy}^2 + \sigma_{yz}^2 + \sigma_{zx}^2)},$$

$$\varepsilon_m = \frac{1}{1 + \nu_s} \sqrt{\frac{1}{2} [(\varepsilon_{xx} - \varepsilon_{yy})^2 + (\varepsilon_{yy} - \varepsilon_{zz})^2 + (\varepsilon_{zz} - \varepsilon_{xx})^2] + 3(\varepsilon_{xy}^2 + \varepsilon_{yz}^2 + \varepsilon_{zx}^2)}, \quad (\text{B.2})$$

where ν_s is the Poisson's ratio (which varies with deformation). Furthermore, the stress tensor σ of the non-linear elastic material is related to the strain tensor ϵ via the usual relation

$$\sigma_{ij} = \frac{\nu_s E_s}{(1 + \nu_s)(1 - 2\nu_s)} \delta_{ij} \epsilon_{kk} + \frac{E_s}{1 + \nu_s} \epsilon_{ij}, \quad (\text{B.3})$$

which, in an inverse fashion, reads

$$\epsilon_{ij} = \frac{1 + \nu_s}{E_s} \sigma_{ij} - \frac{\nu_s}{E_s} \delta_{ij} \sigma_{kk}, \quad (\text{B.4})$$

with E_s the secant stiffness of the material and δ_{ij} the Kronecker delta symbol. When applying a uniaxial stress $\hat{\sigma}_{xx}$ in the x -direction, with the use of Eqs. (B.3) and (B.4) the corresponding stress and strain components are obtained as

$$\begin{aligned} \sigma_{xx} &= \hat{\sigma}_{xx}, & \sigma_{yy} &= \sigma_{zz} = \sigma_{xy} = \sigma_{yz} = \sigma_{zx} = 0, \\ \epsilon_{xx} &= \frac{\hat{\sigma}_{xx}}{E_s}, & \epsilon_{yy} &= \epsilon_{zz} = -\nu_s \epsilon_{xx} = -\frac{\nu_s \hat{\sigma}_{xx}}{E_s}, \\ \epsilon_{xy} &= \epsilon_{yz} = \epsilon_{zx} = 0. \end{aligned} \quad (\text{B.5})$$

Inserting Eq. (B.5) into Eq. (B.2) leads to

$$\begin{aligned} \sigma_m &= \hat{\sigma}_{xx}, \\ \epsilon_m &= \epsilon_{xx} = \frac{\hat{\sigma}_{xx}}{E_s}, \end{aligned} \quad (\text{B.6})$$

showing that the secant stiffness at a certain state of deformation follows from the corresponding uniaxial stress and strain as $E_s = \sigma_m / \epsilon_m$. In addition, the Poisson's ratio for the elasto-plastic material is given by

$$\nu_s = \frac{1}{2} - \left(\frac{1}{2} - \nu \right) \frac{E_s}{E}. \quad (\text{B.7})$$

Note that for the case of linear elasticity the material parameters reduce to $E_s = E$ and $\nu_s = \nu$. Furthermore, in the limit case of ideal plasticity, the secant stiffness approaches zero, $E_s \rightarrow 0$, and the Poisson's ratio goes to $\nu_s \rightarrow 0.5$, reflecting incompressible plastic deformation. In that case, the equivalent strain, Eq. (B.2)₂, turns into the expression commonly used in plasticity: $\epsilon_m = \sqrt{(2/3) \epsilon'_{ij} \epsilon'_{ij}}$, where $\epsilon'_{ij} = \epsilon_{ij} - (1/3) \delta_{ij} \epsilon_{kk}$ represents the deviatoric strain.

Consider now a *plane-strain* state (with the z -direction corresponding to the out-of-plane direction), where the normal stress σ_{xx} and normal strain ϵ_{xx} are the main variables under the specific loading applied (which is representative of the film delamination problems studied in this communication). From Eqs. (B.3) and (B.4) the other stress and strain components under plane-strain conditions are obtained as

$$\begin{aligned} \sigma_{zz} &= \nu_s \sigma_{xx}, & \sigma_{yy} &= \sigma_{xy} = \sigma_{yz} = \sigma_{zx} = 0, \\ \epsilon_{yy} &= -\frac{(\nu_s + \nu_s^2) \sigma_{xx}}{E_s}, & \epsilon_{zz} &= \epsilon_{xy} = \epsilon_{yz} = \epsilon_{zx} = 0. \end{aligned} \quad (\text{B.8})$$

Substituting Eq. (B.8) into Eq. (B.2) gives

$$\begin{aligned} \sigma_m &= \sqrt{\nu_s^2 - \nu_s + 1} \sigma_{xx}, \\ \epsilon_m &= \frac{1}{1 + \nu_s} \sqrt{\epsilon_{xx}^2 + \epsilon_{xx} \frac{\nu_s(\nu_s + 1)}{E_s} \sigma_{xx} + \frac{\nu_s^2(\nu_s + 1)^2}{E_s^2} \sigma_{xx}^2}. \end{aligned} \quad (\text{B.9})$$

Inverting these relations leads to expressions for the normal stress σ_{xx} and strain ϵ_{xx} in terms of the equivalent stress σ_m and strain ϵ_m :

$$\begin{aligned} \sigma_{xx} &= \frac{\sigma_m}{\sqrt{\nu_s^2 - \nu_s + 1}}, \\ \epsilon_{xx} &= \frac{1 + \nu_s}{2} \left(-\frac{\nu_s}{E_s} \sigma_{xx} + \sqrt{4 \epsilon_m^2 - \frac{3 \nu_s^2}{E_s^2} \sigma_{xx}^2} \right). \end{aligned} \quad (\text{B.10})$$

Note that for the limit case $\nu_s = 0$, Eq. (B.10) correctly reduces to $\sigma_{xx} = \sigma_m$ and $\epsilon_{xx} = \epsilon_m$. The relations given by Eq. (B.10) are used in the semi-analytical study for a film delaminating from an elasto-plastic substrate, see Eq. (13) in Section 2.3.1.

References

- Bagchi, A., Lucas, G.E., Suo, Z., Evans, A.G., 1994. A new procedure for measuring the decohesion energy for thin ductile films on substrates. *J. Mat. Res.* 9, 1734–1741.
- Beuth, J.L., 1992. Cracking of thin bonded films in residual tension. *Int. J. Solids Struct.* 29, 1657–1675.
- Beuth, J.L., Narayan, S.H., 1996. Residual stress-driven delamination in deposited multi-layers. *Int. J. Solids Struct.* 33, 65–78.
- Charalambides, P.G., Cao, H.C., Lund, J., Evans, A.G., 1990. Development of a test method for measuring the mixed mode fracture resistance of bimaterial interfaces. *Mech. Mat.* 8, 269–283.
- Charalambides, P.G., Lund, J., Evans, A.G., McMeeking, R.M., 1989. A test specimen for determining the fracture resistance of bimaterial interfaces. *J. Appl. Mech.* 56, 77–82.
- Chen, C., Fleck, N.A., Lu, T.J., 2001. The mode I crack growth resistance of metallic foams. *J. Mech. Phys. Solids* 49, 231–259.
- Cid Alfaro, M.V., Suiker, A.S.J., de Borst, R., 2010. Transverse failure behaviour of fibre-epoxy systems. *J. Comp. Mat.* 44, 1493–1516.
- Cid Alfaro, M.V., Suiker, A.S.J., de Borst, R., Remmers, J.J.C., 2009. Analysis of fracture and delamination in laminates using 3D numerical modelling. *Eng. Frac. Mech.* 76, 761–780.
- Cid Alfaro, M.V., Suiker, A.S.J., Verhoosel, C.V., de Borst, R., 2010. Numerical homogenization of cracking processes in thin fibre-epoxy layers. *Eur. J. Mech. A/Solids* 29, 119–131.
- Delette, G., Laurencin, J., Murer, S., Leguillon, D., 2009. Effect of residual stresses on the propagation of interface cracks between dissimilar brittle materials: Contribution of two and three-dimensional analyses. *Eur. J. Mech. A/Solids* 35, 97–110.
- Freund, L.B., Suresh, S., 2003. *Thin Film Materials - Stress, Defect Formation and Surface Evolution*. Cambridge University Press, Cambridge, U.K.
- Ho, S., Suo, Z., 1993. Tunneling cracks in constrained layers. *J. Appl. Mech.* 60, 890–894.
- Hofinger, I., Oechsner, M., Bahr, H.-A., Swain, M.V., 1998. Modified four-point bending specimen for determining the interface fracture energy for thin, brittle layers. *Int. J. Frac.* 92, 213–220.
- Hutchinson, J.W., Suo, Z., 1992. Mixed mode cracking in layered materials. *Adv. Appl. Mech.* 29, 63–191.
- Jensen, H.M., 1990. Mixed mode interface fracture criteria. *Acta Metal. Mater.* 38, 2637–2644.
- Klingbeil, N.W., Beuth, J.L., 1997. Interfacial fracture testing of deposited metal layers under four-point bending. *Eng. Frac. Mech.* 56, 113–126.
- Nix, W.D., 1989. Mechanical properties of thin films. *Metall. Trans. A* 20, 2217–2245.
- Ramberg, W., Osgood, W., 1943. Description of Stress-Strain Curves by Three Parameters. National Advisory Committee for Aeronautics, Technical Note No. 902.
- Rice, J.R., 1968. A path-independent integral and approximation analysis of strain concentration by notches and cracks. *J. App. Mech. (ASME)* 35, 379–386.
- Rice, J.R., 1988. Elastic fracture concepts for interfacial cracks. *J. Appl. Mech. (ASME)* 55, 98–103.
- Shaviv, R., Roham, S., Woytowicz, P., 2005. Optimizing the precision of the four-point bend test for the measurement of thin film adhesion. *Microelec. Eng.* 82, 99–112.
- Suiker, A.S.J., Fleck, N.A., 2004. Crack tunneling and plane-strain delamination in layered solids. *Int. J. Frac.* 125, 1–32.
- Suiker, A.S.J., Fleck, N.K., 2006. Modelling of fatigue crack tunneling and delamination in layered composites. *Compos. Part A* 37, 1722–1733.
- Turon, A., Camanho, P.P., Costa, J., Davila, C.G., 2006. A damage model for the simulation of delamination in advanced composites under variable-mode loading. *Mech. Mater.* 38, 1072–1089.
- Tvergaard, V., Hutchinson, J.W., 1992. The relation between crack growth resistance and fracture process parameters in elastic-plastic solids. *J. Mech. Phys. Solids* 40, 1377–1397.
- Tvergaard, V., Hutchinson, J.W., 1993. The influence of plasticity on mixed mode interface toughness. *J. Mech. Phys. Solids* 41, 1119–1135.
- Wei, Y., Hutchinson, J.W., 1997. Nonlinear delamination mechanics for thin films. *J. Mech. Phys. Solids* 45, 1137–1159.
- Zhuk, A.V., Evans, A.G., Hutchinson, J.W., Whitesides, G.M., 1998. The adhesion energy between polymer thin films and self-assembled monolayers. *J. Mat. Res.* 13, 3555–3564.